Title: Temporal scaling of dopamine neuron firing and dopamine release by distinct ion channels shape behavior

Authors

Barbara Juarez[1,2,+], Mi-Seon Kong[1], Yong S. Jo[1,§], Jordan E. Elum[1], Joshua X. Yee[1], Scott Ng-Evans[1], Marcella Cline[1], Avery C. Hunker[2,†], Meagan A. Quinlan[1,†], Madison A. Baird[2,‡], Abigail J. Elerding[2], Mia Johnson[1], Derek Ban[1], Adriana Mendez[1%], Nastacia L. Goodwin[3], Marta E. Soden[2], Larry S. Zweifel*[1, 2].

Affiliations

[1]Department of Psychiatry and Behavioral Sciences, University of Washington; Seattle, WA, United States.

[2] Department of Pharmacology, University of Washington; Seattle, WA, United States.

[3] Department of Biostructure, University of Washington; Seattle, WA, United States.

+ Current affiliation: University of Maryland, Baltimore; Baltimore, MD. United States.

§ Current affiliation: School of Psychology, Korea University; Seoul, Republic of Korea.

†Current affiliation: Allen Brain Institute; Seattle, WA, United States.

‡ Current affiliation: Cajal Neuroscience; Seattle, WA, United States

% Current affiliation: Icahn School of Medicine at Mount Sinai, New York, NY, United States

*Corresponding author. Email: larryz@uw.edu

Abstract

Despite the widely known role of dopamine in reinforcement learning, how the patterns of dopamine release that are critical to the acquisition, performance, and extinction of conditioned responses are generated is poorly resolved. Here, we demonstrate that the coordinated actions of two ion channels, Kv4.3 and BKCa1.1, control the pattern of dopamine neuron firing and dopamine release on different time scales to regulate separate phases of reinforced behavior and extinction in mice. Inactivation of Kv4.3 in VTA dopamine neurons increases *ex vivo* pacemaker activity and excitability that is associated with decreased rates of bursting and increased *in vivo* ramping dynamics prior to lever press in a learned instrumental response paradigm. Loss of Kv4.3 enhances performance of the learned response and facilitates extinction. In contrast, loss of BKCa1.1 increases duration of burst firing and phasic dopamine release that enhances learning of an instrumental response. Inactivation of BKCa1.1 also enhances extinction burst lever pressing in early extinction training that is associated with a greater change in activity between reinforced and unreinforced actions. These data demonstrate that disruption of intrinsic regulators of neuronal activity differentially impacts dopamine dynamics observed during reinforcement learning and extinction behaviors.

Teaser

Ion channels in midbrain dopamine neurons are critical for patterning action potential firing, dopamine release, and learning.

MAIN TEXT

Introduction

Reinforcement and extinction learning are essential processes by which an organism links environmental stimuli and actions with outcomes. Dopamine-producing neurons in the ventral

48 tegmental area (VTA) of the midbrain facilitate reinforcement learning to promote the
49 performance of goal-oriented behavior through modulation of information processing in the
50 forebrain, most notably in the nucleus accumbens (NAc) (*1*). Distinct patterns of dopamine release,
51 such as tonic, phasic (burst), or ramping patters, that occur on different time scales during the
52 acquisition, performance, and extinction of a conditioned response are thought to underlie
53 dopamine function within these contexts(*2–6*). Despite the evidence that dopamine is critical for
54 reinforcement learning(*1–3*), how the intrinsic properties of the cell contribute to patterning action
55 potential firing and neurotransmitter release during distinct phases of reinforcement learning is not
56 well resolved. Moreover, recent findings suggest that dopamine release dynamics can occur
57 independently of the activity patterns at the cell body(*5*) raising the possibility that the firing
58 properties of dopamine neurons at the level of the cell body may be dispensable for some aspects
59 of reinforcement learning.

60 VTA dopamine neurons display spontaneous action potential firing in the absence of
61 afferent inputs(*7*) that is regulated by a suite of voltage-gated ion channels (*8–10*). Potassium
62 currents shape the action potential waveform to regulate the frequency and pattern of firing (*8–12*).
63 Kv4.3 subunits contribute to A-type potassium currents (I_A) in dopamine neurons that facilitate
64 repolarization and control the frequency of firing (*9*). BKCa1.1 subunits are the essential subunits
65 of voltage-sensitive, calcium-activated big conductance potassium (BK) channels, which conduct
66 BK currents (I_{BK}). These subunits are expressed in dopamine neurons and conduct currents that
67 mediate the initial phase of the action potential afterhyperpolarization to control the pattern of
68 firing (*10*). Based on the recruitment of these channels during different phases of the action
69 potential repolarization and afterhyperpolarization, we hypothesized that targeted disruption of
70 their function in VTA dopamine neurons would differentially impact action potential firing

71 patterns and neurotransmitter release. Specifically, loss of Kv4.3 would induce more pacemaker-
72 like activity and loss of BKCa1.1 would induce more irregular/burst patterns of activity. Thus,
73 inactivation of these channels provides a means to further resolve whether intrinsic regulators of
74 dopamine neuron action potentials influence activity patterns at the level of the cell body and
75 neurotransmitter release dynamics in terminal fields during reinforcement learning.

76 Using CRISPR/Cas9 gene-editing technologies, we selectively targeted mutagenesis of
77 Kv4.3 (gene name: *Kcnd3*) and BKCa1.1 (gene name: *Kcnma1*) in dopamine releasing neurons of
78 the VTA. We found that inactivation of Kv4.3 and BKCa1.1 differentially affected the action
79 potential waveform, neuronal excitability, and patterns of action potential firing. We further show
80 that loss of function (LOF) of these two channels differentially impacted the acquisition,
81 maintenance, and extinction of a reinforced behavioral response that was associated with distinct
82 effects on the *in vivo* patterns of cell body activity and dopamine release during these behaviors.
83 Specifically, loss of BKCa1.1 ion channel subunits in VTA dopamine neurons enhanced burst
84 firing and phasic dopamine release that was associated with enhanced acquisition of instrumental
85 behavior and a heightened extinction burst behaviors. In contrast, loss of Kv4.3 increased
86 dopamine neuron excitability, decreased burst rates, and increased ramping that was associated
87 with increased performance of a learned response. Further, loss of Kv4.3 also led to facilitated
88 extinction of an instrumental response that was associated with a lack of differential dopamine
89 neuron responses between actions associated with rewarded or omitted outcomes. These findings
90 demonstrate that intrinsic regulators influence patterns of dopamine cell body activity and terminal
91 release dynamics *in vivo* to shape control the behavior during reinforcement and extinction
92 learning.

93 **Results**

94 **CRISPR/Cas9 inactivation of Kv4.3 and BKCa1.1**

95 To determine the distribution of *Kcnd3* and *Kcnma1* expression in the VTA, we performed
96 *in situ* hybridization (RNAscope) to quantify the mRNA levels for these ion channel subunits and
97 the rate-limiting enzyme in dopamine production, tyrosine hydroxylase (*Th)*. We find that Kv4.3
98 and BKCa1.1 subunits are expressed in most dopamine neurons along the rostral-caudal axis of
99 the VTA (Fig. 1, A-C, fig. S1, A-E).

100 To selectively inactivate these two channels, we used a viral-mediated, Cre-inducible
101 CRISPR/SaCas9 system (*13*). Adeno-associated viruses (AAV) containing single guide RNA
102 directed to either of the two loci (AAV1-FLEX-SaCas9-sg*Kcnd3* or AAV1-FLEX-SaCas9-
103 sg*Kcnma1*) were generated (Fig. 1, D and H) and injected into the VTA of separate groups of adult
104 *Slc6a3*(DAT)-IRES-Cre mice (fig. S2, A; fig. S3-S4). Control DAT-IRES-Cre mice received
105 injections of AAV1-FLEX-eYFP into the VTA. We genetically validated gene mutagenesis of
106 targeted sequences by co-injection with AAV-FLEX-KASH-GFP into the VTA and harvesting
107 tissue after four weeks. We found that the AAV mediated Cre-inducible CRISPR/SaCa9 system
108 yielded high efficiency indel formation (Fig. 1, E, I; fig S2 B-C).

109 Next, we used patch-clamp electrophysiology to determine impact of CRISPR/SaCas9
110 induced Kv4.3 or BKCa1.1 gene mutagenesis on channel activity in VTA dopamine neurons. To
111 visualize cells, we co-injected the LOF mice with AAV-FLEX-eYFP. First, we quantified I_A in
112 VTA dopamine neurons in control mice and mice that received AAV1-FLEX-SaCas9-sg*Kcnd3*
113 (Fig. 1, F-G). In control mice, a depolarization protocol induced robust I_A, quantified as the
114 difference between the instant and sustained parts of the generated current; this was nearly
115 abolished after bath application of the I_A inhibitor, AmmTx3, suggesting the presence of I_A (Fig.
116 1, F-G). In mice that received AAV1-FLEX-SaCas9-sg*Kcnd3* in VTA dopamine neurons, we

117 observed almost no I_A in baseline conditions and insensitivity to AmmTx3 (Fig. 1, F-G),
118 suggesting Kv4.3 LOF. We next quantified I_{BK}, a major component of I_K generated after
119 depolarization step, in VTA dopamine neurons of in control mice and mice that received AAV1-
120 FLEX-SaCas9-sg*Kcnma1* (Fig. 1, J-K). In control mice, iberiotoxin, a BK channel-specific
121 inhibitor, significantly reduced maximal peak of I_K when compared to I_K before iberiotoxin bath
122 application, suggesting pharmacological blockade of the BK channel current component in
123 dopamine neurons (Fig. 1, J-K). However, in VTA dopamine neurons from AAV1-FLEX-SaCas9-
124 sg*Kcnma1* injected mice, there was already a significant reduction in I_K under baseline conditions
125 that was not changed after iberiotoxin application, suggesting that there is no iberiotoxin-sensitive
126 BK channel current component following CRISPR injection (Fig. 1, J-K). Using current
127 subtraction methods, we further quantified the specific I_{BK} and found that AAV1-FLEX-SaCas9-
128 sg*Kcnma1* significantly reduced I_{BK} (fig. S4, A-C).

129 It is possible that CRISPR/SaCas9-induced LOF of Kv4.3 or BKCa1.1 channels could
130 impact the expression of related potassium channel subunits to compensate for their loss. *Kcnd2*
131 (Kv4.2), another A-type potassium channel subunit, is also expressed in VTA dopamine neurons
132 in mice (*14*). Mutagenesis of *Kcnd3* did not alter midbrain expression of this subunit (fig. S2, D).
133 Previous studies have found no other pore forming alpha subunits for BK channels in the VTA.
134 However, small-conducting calcium activated potassium channels (SK) are expressed in these
135 cells and contribute to the after hyperpolarization (*15*). We found no differences in *Kcnn3* (SK3)
136 expression in the midbrain following *Kcnma1* mutagenesis (fig. S2, E). These data suggest that
137 LOF of either Kv4.3 and BKCa1.1 has significant and specific impacts on their respective currents
138 without inducing compensatory changes in other related channels.

139 **Kv4.3 and BKCa1.1 regulate *ex vivo* and *in vivo* action potential firing patterns but not *ex***
140 ***vivo* dopamine release from terminals**

141 Next, we profiled the impacts of ion channel subunit LOF on *ex vivo* activity characteristics
142 of VTA dopamine neurons. As predicted, CRISPR/Cas9 induced Kv4.3 LOF altered the dopamine
143 neuron action potential waveform by increasing the action potential half width and slowing
144 repolarization relative to control of spontaneously active action potentials in VTA slices (Fig. 2,
145 A-D). BKCa1.1 LOF cells showed significantly more depolarized afterhyperpolarization
146 compared to control cells (Fig. 2, A-B, E). Dopamine neurons from BKCa1.1 LOF also showed
147 a more depolarized resting membrane potential relative to control cells (Fig. 2, A-B, F). Both
148 Kv4.3 LOF and BKCa1.1 LOF in VTA dopamine neurons significantly depolarized the action
149 potential threshold when compared to control neurons, but neither manipulation affected the peak
150 of the action potential (fig. S4, H-I). These cell-specific CRISPR/Cas9 ion channel subunit LOF
151 changes were different compared to the less specific pharmacological blockade of Kv4 and BK
152 channels, supporting the use of CRISPR for this study (fig. S4, E-G). To determine if the changes
153 we observed in action potential shape from spontaneously action potentials in Kv4.3 LOF and
154 BKCa1.1 LOF dopamine neurons were impacted by the depolarized resting membrane potential,
155 we clamped the neurons at -60 mV and injected current to induce action potential firing (fig S4,
156 J). We found similar effects on action potential shape, although notably no significant change in
157 the anti-peak of the afterhyperpolarization in BKCa1.1 LOF neurons was observed, though the
158 shape of the afterhyperpolarization was affected (fig S4, J-N).

159 Given the changes in action potential waveform dynamics associated with Kv4.3 LOF and
160 BKCa1.1 LOF, we sought to establish whether these perturbations affect neuronal excitability and
161 patterns of action potential firing. Input-output analysis (excitability) of action potential firing

162 following depolarizing current injection from cells held at -60 mV (Fig. 2, G-H) and cells at resting
163 membrane potential (fig. S4, O) revealed that Kv4.3 LOF in VTA dopamine neurons increased
164 neuronal excitability when compared to control cells. Further, the frequency of spontaneous action
165 potential firing in Kv4.3 LOF cells is greater relative to control cells (Fig. 2, I-J; fig. S4, P). In
166 contrast, BKCa1.1 LOF did not affect these parameters (Fig. 2 G-J; S4, O). However, BKCa1.1
167 LOF did shift the pacemaker-like *ex vivo* activity observed in control and Kv4.3 LOF cells to a
168 more irregular pattern, as evidenced by an increase in the coefficient of variation in the inter-spike
169 interval (CV-ISI) (Fig. 2, I-K; fig. S4, P).

170 Increased CV-ISI in VTA dopamine neurons of BKCa1.1 LOF mice is consistent with a
171 shift to more burst-like activity (*11*); however, this pattern of firing by dopamine neurons is most
172 accurately assessed by recording neural activity *in vivo*. To identify putative dopamine neurons
173 during *in vivo* recording under baseline conditions or during behavior from mice that received
174 control virus or CRISPR viruses for Kv4.3 LOF or BKCa1.1 LOF, we combined CRISPR/Cas9
175 mutagenesis with cell-type specific expression of channelrhodopsin (ChR2), *in vivo* single-unit
176 electrophysiology using optetrode microdrives implanted in the VTA (fig. S5, A-C) (*11,16*). To
177 optogenetically identify putative dopamine neurons, ChR2 was optically stimulated using 10
178 pulses of blue light at a frequency of 20 Hz repeated 20 times at the end of a recording session; if
179 action potential activity was induced in a time-locked manner, it was categorized as an optically-
180 sensitive putative dopamine neuron (*11*, *16*). We first analyzed the baseline properties of putative
181 dopamine neurons to understand how VTA dopamine activity is altered after CRISPR/Cas9 LOF.
182 Overall firing rate did not differ between the cell groups (fig. S5, D). The number of burst events
183 per second (burst rate) and the percentage of spikes fired in bursts was similar between control and
184 BKCa1.1 LOF cells but was significantly reduced in Kv4.3 LOF cells relative to controls (Fig. 2L;

185 fig. S5, E). In contrast, the duration of the burst events and the number of spikes fired in a burst
186 were significantly increased in BKCa1.1 LOF mice relative to controls but were unaffected in
187 Kv4.3 LOF cells (Fig. 2, M; fig. S5, F). Together, these findings indicate that Kv4.3 LOF in VTA
188 dopamine neurons reduces burst activity while BKCa1.1 LOF increases burst duration when burst
189 activity is induced.

190 In addition to regulating action potentials at the cell body, potassium channels also regulate
191 neurotransmitter release (*17*, *18*). To address whether Kv4.3 or BKCa1.1 LOF function impacts
192 terminally evoked dopamine release dynamics independent from cell body firing, we injected
193 CRISPR/SaCas9 viruses into the VTA along with the redlight-shifted opsin Chrimson (*19*) and
194 injected the genetically encoded dopamine sensor dLight1.3b (*5*) into the NAc (Fig. 2, N). After at
195 least 4 weeks, we performed *ex vivo* 2-photon slice imaging of optically evoked dopamine release
196 in acute brain slices containing the NAc, where VTA dopamine cell bodies are not present. This
197 *ex vivo* preparation helped us determine if there are any terminal-specific channel subunit LOF
198 effects on dopamine release, dissociating it from impacts of cell body LOF. VTA dopamine
199 terminals present in the NAc that express Chrimson were optically stimulated (1 s) at different
200 frequencies (1, 5, 10, and 20 Hz) while imaging dLight fluorescence (Fig. 2, N). We did not detect
201 differences between control and Kv4.3 LOF or BKCa1.1 LOF mice (Fig. 2, O-P). These findings
202 suggest that CRISPR induced Kv4.3 LOF and BKCa1.1 LOF have primary effects at the cell body.

203 **Kv4.3 and BKCa1.1 differentially regulate instrumental behavior**

204 To assess whether Kv4.3 and BKCa1.1 LOF impacts reinforcement learning, we first
205 trained mice in an appetitive Pavlovian conditioning paradigm where a lever extension followed
206 by retraction (10 s, CS) signals reward (Rew) delivery (Fig. 3A). We did not observe behavioral
207 differences between Kv4.3 LOF and BKCa1.1 LOF mice relative to controls during the CS

208 presentation or ITI period (Fig. 3, B-C). Learning, as assessed by the conditioned approach (CS
209 head entry rate minus ITI head entry rate) was also not different between controls and LOF groups
210 (Fig. 3, D).

211 Following Pavlovian conditioning, mice were transitioned to a fixed-ratio (FR1) schedule
212 of operant reinforcement learning in which lever retraction and reward delivery were contingent
213 on a lever press action (LP) (Fig. 3, E). BKCa1.1 LOF learned the contingency faster than control
214 mice on day 1 of training (Fig. 3, F, G left). Control and Kv4.3 LOF mice increased responding
215 between the first and second day that remained elevated on the third day, with no differences in
216 total lever presses between them (Fig. 3, F, G left). However, Kv4.3 LOF mice had a higher initial
217 rate of responding than control mice on the third day, once the task was acquired (Fig. 3, G, right).
218 Analysis of lever press ethograms during the early (first 30 minutes) or late (last 30 minutes) halves
219 of the session shows the known distribution of individual variability in LP behavior in control mice
220 on the first day (Fig. 3, H, J). We also determined inter-press interval timing across groups (Fig.
221 3, I, K). This all revealed differences in the pattern of lever pressing between the control and LOF
222 groups (Fig. 3, H-K). BKCa1.1 LOF mice started pressing more quickly with a shorter inter-press
223 interval on the first day when compared to controls, consistent with the faster learning of the
224 contingency (Fig. 3, H-I). Once the contingency was learned, control and BKCa1.1 LOF mice had
225 a relatively stable level of responding on the third day; however, Kv4.3 LOF mice showed a high
226 level of responding in the first half of the session that diminished in the second half when compared
227 to controls (Fig. 3, G right, J-K), suggesting an enhanced invigorated performance of the task.

228 Differences in reinforcement learning were not associated with changes in overall
229 locomotor activity (fig. S6, A-B). To determine if Kv4.3 LOF or BKCa1.1 LOF can result in
230 alterations in baseline anxiety, we performed an open field test and elevated plus maze and found

231 no differences between controls and CRISPR LOF groups (fig. S6, C-F). To assess whether the
232 differences in operant responding reflected altered motivation, we assayed mice in a progressive
233 ratio schedule of reinforcement. We did not observe differences between the groups in this task
234 (fig. S6, G).

235 **Kv4.3 and BKCa1.1 differentially regulate behaviorally-evoked firing patterns and**
236 **dopamine release**

237 Differential regulation of action potential waveforms, intrinsic excitability, *in vivo* cell
238 body activity patterns at baseline, and patterns of instrumental behavior suggest that Kv4.3 LOF
239 and BKCa1.1 LOF can cause distinct changes in the encoding of reward-related behaviors. To test
240 this, we performed *in vivo* electrophysiology during the instrumental conditioning task with optical
241 and pharmacological identification of VTA dopamine neurons (Fig. 4, A-B; fig. S5, C) following
242 Pavlovian conditioning as above. Due to the restrictive nature of the tethering for recording, all
243 tethered mice underwent 5 days of FR1 to reach similar behavioral performances as untethered
244 mice and cell body activity was measured on day 1 and day 5 (fig. S6, H-J). Recordings were
245 performed throughout the entire behavioral session which was followed by delivery of blue light
246 for optical identification and injection of quinpirole, a dopamine D2 receptor agonist, to identify
247 putative dopamine neurons. Although it is difficult to glean much information regarding the action
248 potential waveform from extracellular recordings because of the unknown distance from the
249 electrode and the recorded cells, we did observe qualitative differences in the waveforms of light-
250 sensitive cells from Kv4.3 LOF and BKCa1.1 LOF mice relative to cells from controls (fig. S5,
251 G) that were similar to those observed in whole cell recordings. The overall firing rates of
252 individual cells surrounding the lever press and reward delivery period were variable, but clear
253 differences in the patterns of activity were evident (fig. S7, A-D). In lever press responsive cells,

254 the mean firing rate during the baseline period prior to lever press did not differ on the first day of
255 FR1 reinforced learning (fig. S7, A) but was significantly elevated in Kv4.3 LOF mice relative to
256 controls on the fifth day (fig. S7, D). To account for the overall variance in firing rate, cell activity
257 was normalized using a Z-score (Fig. 4, C). Analysis of the area under the curve (AUC) of the Z-
258 score following lever press revealed significantly larger responses to the lever press in BKCa1.1
259 LOF cells relative to controls on both days (Fig. 4, D). In contrast, we observed significantly
260 reduced responses in Kv4.3 LOF mice relative to controls on day 5 following reward delivery (Fig.
261 4, E).

262 To determine whether changes in behaviorally-evoked action potential firing at the cell
263 body associated with ion channel LOF is related to dopamine release dynamics downstream, we
264 expressed dLight1.3b in the NAc of Kv4.3 LOF, BKCa1.1 LOF, and control mice (fig. S8) and
265 performed fiber photometry during FR1 following Pavlovian conditioning as above. Again,
266 tethered mice underwent 5 days of FR1 instead of 3 days (fig. S6 H-J) and dopamine signals were
267 measured on day 1 and day 5. Control mice showed phasic increases in dopamine time-locked to
268 LP and Rew on day 1 (Fig. 5, A top row) and day 5 (Fig. 5, A middle row, bottom row). Kv4.3
269 LOF mice showed LP and Rew dopamine signals on the first day (Fig. 5, A top row) and day 5
270 (Fig. 5, A middle row, bottom row heat maps). BKCa1.1 LOF mice had large dopamine release
271 events to LP and Rew on day 1 (Fig. 5, A top row) and day 5 (Fig. 5, A middle row, bottom row).
272 Similar to cell body firing, BKCa1.1 LOF mice had larger dLight1.3b signals during LP on day 1
273 when compared to controls (Fig. 5, B). Rew-evoked signals were also significantly higher in
274 BKCa1.1 LOF mice on both days compared to controls (Fig. 5, C). Although phasic increases were
275 more prominent in BKCa1.1 LOF mice, we found ramping of the dLight1.3b signal prior to the

276 lever press on day 5 was increased in Kv4.3 LOF mice relative to controls. (Fig. 5, D-E). This was
277 also evident in the firing rates of Kv4.3 LOF mice relative to controls (fig. S7, E).

278 **Kv4.3 and BKCa1.1 LOF differentially regulates extinction of an operant response**

279 Following Pavlovian and FR1 conditioning, a subset of mice underwent extinction training
280 with reward omission (Fig. 6, A). Control mice exhibited an extinction burst in lever pressing on
281 the first day of extinction (higher pressing on day 1 of extinction versus the last day of reinforced
282 FR1 conditioning). This extinction burst was elevated in BKCa1.1 LOF mice relative to control
283 mice (Fig. 6, B-C; fig. S9, A-C). In contrast, Kv4.3 LOF mice displayed potentiated extinction, as
284 evidenced by the significantly reduced lever presses during the first day of extinction training
285 relative to control mice (Fig. 6, B-C; fig. S9, A-C). These differences in extinction burst behaviors
286 are also represented using a ratio of lever presses on the first day of extinction compared to the last
287 day of reinforced FR1; ratios greater than indicate an induction of an extinction burst, as observed
288 in control mice and BKCa1.1 mice, to a greater degree (fig. S9, G). Notably, Kv4.3 LOF mice do
289 not have this difference (fig. S9, G). The number of lever presses in BKCa1.1 LOF and control
290 mice decreased during the extinction session but remained relatively stable in Kv4.3 LOF mice
291 (Fig. 6, C; fig S9, A-B). All mice performed similarly on the last day of extinction (Fig. 6, B; fig.
292 S9, D-F).

293 We were intrigued by the observation that BKCa1.1 mice showed an elevated extinction
294 burst and that Kv4.3 mice showed a reduced extinction burst relative to controls. Because BKCa1.1
295 mice have faster acquisition of the FR1 instrumental response, we asked whether there is a
296 relationship between responding on day 1 of acquisition and day 1 of extinction. We found a
297 significant positive correlation between the level of responding on acquisition day 1 and extinction

298 day 1, suggesting that mice that learn the task faster have the largest extinction burst responses
299 with reward is omitted (fig. S9, H).

300 The altered extinction behaviors observed in Kv4.3 LOF and BKCa1.1 LOF mice may be
301 due to differences in dopamine neuron activity and release between actions of reinforced and
302 omitted outcomes. To explore this further, we compared the normalized action potential firing (Z-
303 score) and dopamine release patterns during the lever press period of the mice during the first day
304 of learning in the FR1 reinforced conditioning presented in Fig. 4 and Fig. 5 and the first day of
305 FR1 extinction (reward omitted) (Fig. 6, D). All groups showed general reductions in putative
306 dopamine neuron action potential firing and dlight1.3b signals during extinction. In control mice
307 normalized firing was reduced, but we observed no significant differences in cell body activity
308 (Fig. 6, E left). However, dLigh1.3b signals in the NAc of control mice on Extinction day 1 were
309 significantly reduced when compared to signals from reinforced FR1 learning (Fig. 6, E right).
310 Kv4.3 LOF mice, which display control-like acquisition of the reinforced task and reduced lever
311 pressing during, showed no differences between days in VTA dopamine cell body activity and
312 dLight1.3b signals in the NAc (Fig. 6, F). Of note, we found that the overall firing rate of lever
313 press responsive cells in the Kv4.3 LOF mice during the pre-lever press period was elevated
314 relative to control mice (fig. S10, A-B), and the overall pattern of activity was remarkably similar
315 to what we observed on the first day of conditioning (compare fig. S7 to fig. S10). BKCa1.1 LOF
316 mice, which have potentiated learning of reinforced task and a larger extinction burst, displayed
317 significant reductions in both VTA dopamine cell body activity and dLight1.3b signals in the NAc
318 on the first day of extinction training when compared to FR1 reinforced Day 1 (Fig. 6, G).

319

320 **Discussion**

321 Our results show that LOF of ion channels that contribute to the generation of the action
322 potentials alters the patterns of dopamine neuron firing and dopamine release to influence
323 reinforcement learning, performance, and extinction. Using viral delivery of CRISPR/SaCas9 we
324 were able to generate high-efficiency mutagenesis that allowed us to determine the cell-type
325 specific function of Kv4.3 and BKCa1.1 subunits in VTA dopamine neurons of the adult brain.
326 We found that CRISPR/SaCas9 mutagenesis of *Kcnd3* (Kv4.3 LOF) effectively reduced the
327 AmmTx-sensitive A-type potassium current and mutagenesis of *Kcnma1* (BKCa1.1 LOF)
328 significantly attenuated the iberiotoxin-sensitive BK current. Loss of these channels altered the
329 action potential waveform by broadening the action potential half-width (Kv4.3 LOF) and
330 reducing the AHP (BKCa1.1 LOF). Reduced AHP in VTA dopamine neurons following loss of
331 BKCa1.1 is distinct from the effects of inhibition of BK current in substantia nigra pars
332 compacta (SNc) dopamine neurons where a paradoxical increase in afterhyperpolarization was
333 reported (*10*). This could be due in part to the higher expression of the small conductance
334 potassium channel, SK3 in SNc dopamine neurons (*20*) that also contributes to the
335 afterhyperpolarization (*15*), or the reciprocal interactions between Kv2 channels and BK
336 channels in SNc dopamine neurons (*10*).

337 Kv4.3 LOF resulted in an increase in VTA dopamine neuron excitability and pacemaker
338 activity, as would be predicted based on the recruitment of A-type potassium channel
339 conductance during the rapid depolarization phase of the action potential to generate rapid
340 feedback and allow for slow pacemaker activity (*9*). Loss of BKCa1.1 resulted in irregular action
341 potential firing in VTA dopamine neurons *ex vivo* and prolonged burst events in these cells *in*
342 *vivo*. This *ex vivo* result again contrasts to the effects observed in SNc dopamine neurons, likely
343 relating to the differential effects on the AHP. Reduced AHP following BKCa1.1 LOF reported

344 here is similar to that observed following inhibition of BK in cerebellar Purkinje cells that also
345 increased burst firing (*21*). Based on these observations, we propose that BKCa1.1 channels
346 terminate burst events through regulation of the action potential afterhyperpolarization in VTA
347 dopamine neurons, and in their absence, phasic dopamine is enhanced once a burst is initiated,
348 which assigns a higher value to action. This facilitates the acquisition of the conditioned
349 response and establishes a greater differential response during extinction thus, generating a larger
350 extinction burst (*2*, *3*, *22*, *23*).

351 We find that Kv4.3 channels regulate firing frequency in acute brain slice preparations,
352 likely through the regulation of membrane repolarization (*9*). However, we did not observe
353 changes in baseline firing rate *in vivo*, likely due to the influence of GABAergic inhibition in the
354 intact VTA. Intriguingly, on the last day of FR1 conditioning and the first day of extinction
355 training, we observed significantly higher baseline firing rates in lever press responsive cells.
356 We hypothesize that this increased activity is a reflection of a reduction in the inhibitory tone on
357 these cells following learning, such as through disinhibition (*24*), that elevates tonic activity.
358 Indeed, it has previously been shown that when tonic signals such as ramping are elevated
359 performance of a learned response is enhanced (*3–6*). In contrast to previous reports that ramping
360 of dopamine release occurs independent of activity at the cell body (*5*), our data suggest that the
361 intrinsic excitability of the cell, regulated by Kv4.3, contributes at least partially to this process
362 in reinforced trials. During the first day of extinction training, Kv4.3 LOF mice had a lower
363 extinction behavior burst than control or BKCa1.1 LOF mice. We also observed that Kv4.3 LOF
364 did not display significant changes in dopamine release of action potential firing between the
365 first day of acquisition and the first day of extinction. In contrast, BKCa1.1 mice showed the
366 largest difference between these two days. This suggests that the level of extinction burst is

367 likely related to the perceived value of the action. BKCa1.1 mice had the largest phasic increase
368 to the lever press during acquisition and the smallest response during extinction; thus, generating
369 the largest difference between the reinforced and unreinforced actions. In contrast, Kv4.3 LOF
370 mice showed prominent ramps at the cell body and in terminal function but reduced phasic
371 responses that resulted in a loss of significant differences between the responses during
372 reinforced and unreinforced trials.

373 A limitation of the current study relating to the loss of function of Kv4.3 and BKCa1.1 is
374 the potential impact on conductance associated with other ion channels and extrinsic signaling.
375 Indeed, as mentioned above, BK currents can influence Kv2 currents, and vice versa in SNc
376 dopamine neurons (*9*). Because Kv4 channels are activated during rapid ramping of the
377 depolarization they help to constrain the inward sodium current; thus, their loss would be
378 predicted to result in a larger sodium conductance and higher frequency firing (*9*). In VTA
379 dopamine neurons a small subthreshold sodium current has also been shown to contribute to
380 pacemaker activity (*23*), reducing the resting potential to varying degrees following Kv4.3 or
381 BKCa1.1 mutagenesis could disrupt the subthreshold sodium conductance and alter the
382 excitability of VTA dopamine neurons or their pacemaker activity. These studies highlight the
383 critical interactions between ion channels that work collectively to regulate action potential
384 firing. Further, these ion channels and their respective currents have been previously identified to
385 have cooperative or opposing roles beyond voltage-gated intrinsic regulation. For example, I_A is
386 a critical effector of 2-AG modulation of excitability and I_{BK} has been demonstrated to couple to
387 ligand-gated glutamate receptors to regulate synaptic signaling (*34, 35*). Regardless of the
388 mechanism(s) that underlies the impact of Kv4.3 and BKCa1.1 LOF on VTA dopamine neuron
389 physiology, we find significant effects on the action potential waveform, action potential firing

390 both *ex vivo* and *in vivo*, and changes in dopamine release dynamics that supports the importance
391 of their cell autonomous function in these cells.

392 Although we focused on Kv4.3 and BKCa1.1 in dopamine neurons, these channels are
393 expressed widely throughout the brain where they likely serve similar functions in patterning
394 transmitter release. Further, there are numerous other ion channels that contribute to the action
395 potential. The emergence of many of these ion channels as hotspots of missense mutation in
396 neurodevelopmental disorders (*15*) reinforces the importance of understanding how these
397 channels influence cellular and systems function.

398

399 **Materials and Methods**
400
401 **Experimental Design:**

402 **Mice:** All procedures were approved and conducted in accordance with the guidelines of the
403 University of Washington's Institutional Animal Care and Use Committee (Protocol ID: 4249-
404 01). Mice were housed on a 12:12 light: dark cycle with *ad libitum* access to food and water,
405 except when undergoing food restriction for Pavlovian and operant behavioral conditioning.
406 Approximately equal numbers of male and female mice were used, starting at 6-10 weeks of age.
407 Mice were group-housed (2-5 mice per cage), except during night-day locomotion assays. Either
408 C57BL/6J (Jackson Laboratory for *in situ* hybridization with RNAscope) or *Slc6a3*-IRES-Cre
409 (DAT-IRES-Cre (Jackson Laboratory, Jax 006660, backcrossed to C57BL/6J) mice were used.

410

411 **Viruses:** All adeno-associated viruses (AAV) were produced in-house with titers of 1-3X10^{12}
412 particles mL^{-1}, as described (*25*). Cre-inducible CRISPR viruses: AAV1-CMV-FLEX-SaCas9-
413 HA-U6-sgKcnd3, AAV1- CMV-FLEX-SaCas9-HA-U6-sgKcnma1. Cre-inducible optogenetic

414 viruses: AAV1- EF1α-FLEX-ChR2-eYFP and AAV1- EF1α-FLEX-Chrimson-TdTomato.
415 Dopamine sensor virus: AAV1-CAG-dLight1.3B. Cre-inducible control and fluorescent virus:
416 AAV1-EF1α-FLEX-eYFP. Cre-inducible FACS virus: AAV1-hSyn1-FLEX-KASH-GFP.
417
418 **CRISPR/Cas9 design:** sgRNAs were designed using methods previously described (*13*, *26*). 21
419 bp sgRNAs for *Kcnd3* (Forward: GAGCGCTATCCCGACACCTTG; Reverse:
420 CAAGGTGTCGGGATAGCGCTC) and *Kcnma1* (Forward:
421 GTCTAGGCTGAGATGGTTCGC; Reverse: GCGAACCATCTCAGCCTAGAC) were
422 generated (Invitrogen) and cloned into pAAV-CMV-FLEX-SaCas9-U6sgRNA for generation of
423 AAVs in house.
424
425 **Surgeries:** DAT-IRES-Cre mice were 6-8 weeks of age at time of surgery, except for mice used
426 for *in vivo* electrophysiology which were at least 10 weeks of age at time of surgery. Mice were
427 anesthetized with isoflurane in a chamber and then placed and secured into the stereotax with
428 isoflurane delivery through a nose cone. For all implants, an anchoring screw was driven into the
429 skull away from the implant site. Mice received eYFP (control), CRISPR/eYFP (*in vitro*
430 electrophysiology or behavioral groups), CRISPR/KASH-GFP (sequencing), or CRISPR/ChR2
431 (*in vivo* electrophysiology) bilateral injections into the VTA (in mm, relative to bregma: A/P: -
432 3.3; M/L ± 0.5; D/V: -4.9 → -4.4), total volume 0.5 µL into each side. A/P coordinates were
433 adjusted for Bregma-Lambda distances using a correction factor of 4.21 mm. For D/V, the
434 syringe was lowered to the deepest indicated coordinate and then raised at the start of the
435 injection. For *ex vivo* two-photon dLight experiments, all mice received a bilateral injection of
436 dLight1.3b into the NAc (in mm, relative to bregma: A/P: +1.42; M/L ± 0.9; D/V: -4.5→-4.1)

437 followed by bilateral VTA injections of CRISPR and Chrimson (0.5 µL each side; control mice
438 received Chrimson viruses diluted to the same ratio). For *in vivo* fiber photometry of dLight,
439 mice received control or CRISPR viruses bilaterally into the VTA and then were injected
440 unilaterally with dLight1.3b into the NAc (in mm, relative to bregma: A/P: -+1.43; M/L - 0.9;
441 D/V: -4.5→-4.1), total volume 0.5 µL; a photometry fiber purchased from Doric (400 µm optical
442 fiber, 1.25 mm metal ferrule) was lowered to D/V -4.1 mm. Fibers were secured to the skull with
443 Metabond (Parkell) and dental cement (Lang Dental). For *in vivo* electrophysiology, microdrives
444 were constructed in-house with a Neuralynx EIB (EIB-16) mounted on a 3D printed L-frame
445 (Applied Rapid Technologies). Each microdrive contained in house constructed optetrodes of an
446 in house constructed optic fiber (200 µm fiber bore and 1.25 mm ceramic ferrule, Precision Fiber
447 Products) and an in-house constructed tetrode bundle of tungsten wire (each tetrode was 4 wires
448 25 mm diameter spun together and heat-sealed, California Fine Wire). After virus injection for
449 CRISPR/ChR2 mixture, a window was created in the skull and the microdrive was lowered to
450 above the VTA (-3.8 mm). Optetrode microdrives were secured to the skull with Metabond and
451 dental cement.
452
453 ***In situ* hybridization using RNAscope:** Wildtype C57BL/6 male and female mice (8-9 weeks
454 old) were used to map ion channel expression in the VTA using RNAscope (ACDBio) (*27*).
455 Brains were flash frozen in 2-methylbutane, and stored at -80°C. VTA sections were collected
456 and processed for RNAscope (20 um, coronal). Representative sections that spanned the VTA
457 were selected for hybridization (A/P in mm: rostral: -3.1; intermediate: -3.5; caudal: -3.8;
458 according to the Paxinos atlas). Sections were prepared for hybridization per manufacturer's
459 (Advanced Cell Diagnostics, Inc) instructions using probes for *Th* (Mm-*Th*), *Kcnd3* (Mm-*Kcnd3*-

460 C3), and *Kcnma1* (Mm-*Kcnma1*-C2). Slides were coverslipped with Fluoromount with DAPI
461 (Southern Biotech) and imaged using a confocal fluorescent microscope (University of
462 Washington Keck Center (NIH grant S10 OD016240), Leica SP8X confocal). Images for each
463 RNAscope experiment were collected using the same acquisition settings for each slide. Analysis
464 was performed on Cell Profiler 4.1.3 (https://github.com/CellProfiler/CellProfiler) using a
465 modified image analysis pipeline for RNAscope (*28*).
466
467 **Immunohistochemistry for target validation:** Following completion of experiments, all mice
468 were checked for viral targeting or implant placement. Mice were deeply anesthetized with
469 Buthenesia and transcardially perfused with cold 1X PBS followed by cold 4%
470 paraformaldehyde (PFA, Sigma-Aldrich). Implants were removed from mice used in *in vivo*
471 electrophysiology or fiber photometry experiments. Brains were post fixed for 24 hours in PFA
472 at 4°C, then moved to 30% sucrose in PBS until cryosectioning occurred. All cryosections were
473 stored in 1X PBS with 0.3% Sodium Azide (Sigma-Aldrich) until immunohistochemistry. For
474 colocalization validation and behavioral experiments, the VTA was coronally sectioned at 30
475 µm. For *in vivo* electrophysiology experiments, the VTA was coronally sectioned at 60 µm. For
476 *in vivo* dLight fiber photometry experiments, coronal sections of the NAc (60 µm) and the VTA
477 (30 µm) were obtained. For *ex vivo* dLight slice experiments, the part of the brain containing the
478 VTA was blocked at the same time as obtaining NAc slices for slice imaging. The block was
479 post-fixed overnight in 4% PFA at 4°C. They were then transferred to 30% sucrose in PBS for at
480 least 24 hours and then VTA slices were cryosectioned at 30 µm. NAc slices (250 µm) used in
481 dLight slice two-photon imaging were immediately transferred to 4% PFA after recording and
482 were fixed overnight at 4°C. Slices were then transferred to 1X PBS until the day of

483 immunohistochemistry. Free floating immunohistochemistry experiments were performed using
484 the following antibodies as needed: rabbit anti-HA (Sigma, cat#: H6908), mouse anti-TH
485 (Millipore, cat#: MAB318), mouse anti-dsred (Takara, cat#: 632496), rabbit anti-GFP
486 (Proteintech, cat#: 50430-2-AP), and chicken anti-GFP (Aves, cat#: GFP-1020) to target
487 CRISPR, TH, Chrimson-TdTomato, Chr2-eYFP, or dLight1.3-GFP viruses followed by
488 secondary antibody application (JacksonImmuno, cat#s: 703-545-155, 711-165-152, 711-165-
489 152, 711-165-152). Sections were placed on slides, coverslipped with Fluoromount with DAPI,
490 and kept in the dark at 4°C until the day of imaging. Images were collected at the UW Keck
491 Center or on a Keyence Fluorescence Microscope (Keyence). Quantification of co-labeled cells
492 for immunohistochemistry was performed using ImageJ 1.53 Cell Counter/Multi-point tool.
493
494 **Fluorescence-activated cell sorting and targeted deep sequencing:** Procedures were
495 performed as previously described (*13*, *26*). AAV1-hSyn1-FLEX-EGFP-KASH and CRISPR
496 viruses (AAV1-CMV-FLEX-SaCas9-U6-sgRNA) targeting either *Kcnd3* or *Kcnma1* were
497 stereotaxically co-injected into the VTA of DAT-IRES-Cre mice. Four weeks after surgery, the
498 VTA of each mouse was extracted, flash frozen in liquid nitrogen, and stored at -80ºC. On day of
499 FACS, VTA tissue from 5 mice per experimental group were combined into a single sample and
500 homogenized in buffer containing (in mM): 320 Sucrose (sterile filtered), 5 CaCl (sterile
501 filtered), 3 Mg(Ac)2 (sterile filtered), 10 Tris pH 7.8 (sterile filtered), 0.1 EDTA pH 8 (sterile
502 filtered), 0.1% NP40, 0.1 Protease Inhibitor Cocktail (PIC, Sigma), 1 β-mercaptoethanol. Nuclei
503 were isolated by centrifugation in 29% iso-osmolar Optiprep solution. GFP+ and GFP- nuclei
504 were sorted using a BD AriaFACS III (University of Washington Pathology Flow Cytometry
505 Core) into a PCR tube strip containing 3 µL of REPLI-g Advanced Single Cell Storage buffer

506 (Qiagen). Whole genome amplification (WGA) was performed directly following FACS using
507 the REPLI-g Advanced DNA Single Cell Kit (Qiagen) according to manufacturer's instructions.
508 For generation of amplicons, samples were amplified (PCR 1) with Phusion High Fidelity
509 Polymerase (Thermo Fisher) followed by reamplification (PCR 2) with a second set of primers.
510 The amplicons were gel extracted using the MinElute gel extraction kit (QIAGEN) and sent to
511 Genewiz for Sanger and amplicon sequencing (Amplicon-EZ). The following primer sets were
512 used to generate <300bp amplicons: PCR 1: *Kcnd3* forward: CATTGGATGGATGCCAGT;
513 *Kcnd3* reverse: GAGGATGCCATAGAAGGC; *Kcnma1* forward:
514 GCAACATGGCTGTTGATG; *Kcnma1* reverse: ACCTCCATGGTCACCGGT. PCR 2: *Kcnd3*
515 forward: TAGCTCCAGCGGACAAGA; *Kcnd3* reverse: CAGAGATGCATTCATAGC;
516 *Kcnma1* forward: CCATTGCTAGCTATGGCA; *Kcnma1* reverse:
517 ATGAGCGCATCCATCTTG.
518
519 **Quantitative PCR (qPCR):** qPCR was utilized to determine mRNA expression of relevant
520 potassium channel subunits in the VTA of control, Kv4.3 LOF and BKCa1.1 LOF mice. Four
521 weeks after CRISPR injection, tissue punches containing the VTA (bilateral) were collected and
522 immediately frozen on dry ice, prior to storage at -80°C. RNA isolations were conducted from
523 tissue samples using Qiagen RNeasy Micro Kit (Qiagen, Catalog no. 74004) according to the
524 manufacturer's instructions. The RNA quality and concentration was assessed for each sample
525 spectrophotometrically (A260/A280 & gt;1.9) by a NanoDrop instrument. Then 100 ng of RNA
526 was reverse transcribed by PCR using SuperScript IV VILO (Invitrogen, Catalog no. 11755050).
527 qPCR was conducted on the cDNA using a Taqman Gene Expression assay consisting of the
528 Taqman Gene Expression Master Mix, and the appropriate Taqman probes in FAM channel

529 (Master Max: Thermo Fisher Scientific, Applied Biosystems, catalog no. 4369016, Taqman
530 probes: *GAPDH* (Assay ID: Mm99999915_g1; Cat. number: 4448489), *En1* (Assay ID:
531 Mm00438709_m1_g1; Cat. number: 4448892), *Th* (Assay ID: Mm00447557_m1_g1; Cat.
532 number: 4331182), *Kcnn3* (Assay ID: Mm00446516_m1; Cat. number: 4448892) and *Kcnd2*
533 (Assay ID: Mm01161732_m1; Cat. number: 4448892). All qPCRs were performed in triplicates
534 and run on an Agilent Technologies MX3005P qPCR machine at 50°C for 2 mins, 95°C for 20 s,
535 then 95°C for 3 s and 60°C for 30 s for 40 cycles. The threshold cycle (Ct value) of each gene
536 was then normalized to GAPDH. ΔCT values were calculated by subtracting the geometric mean
537 of CT values for *Gapdh*, *En1*, and *Th* from the CT values of the gene of interest (*Kcnd2* or
538 *Kcnn3*). Control ΔCT values for the gene of interest were subtracted from the ΔCT values of the
539 experimental group to generate ΔΔCTs. Fold change was calculated as 2^-(ΔΔCT).
540
541 **Slice preparation for *ex vivo* physiology:** Mice injected with CRISPR/eYFP or
542 CRISPR/Chrimson/dLight1.3b were allowed 4-5 weeks recovery after surgery to allow for viral
543 expression, mutagenesis, and residual protein turnover. All solutions were continuously bubbled
544 with O_2/CO_2. Coronal brain slices containing the VTA (200 µm for VTA physiology) or NAc
545 (250 µm for dLight slice two-photon imaging) were prepared in a slush NMDG cutting solution
546 (in mM: 92 NMDG, 2.5 KCl, 1.25 NaH_2PO_4, 30 $NaHCO_3$, 20 HEPES, 25 glucose, 2 thiourea, 5
547 Na-ascorbate, 3 Na-pyruvate, 0.5 $CaCl_2$, 10 $MgSO_4$, pH 7.3–7.4 (*29*). Slices recovered for ~12
548 min in the same solution in a 32°C water bath. Slices were then transferred to a room
549 temperature HEPES-aCSF solution (in mM: 92 NaCl, 2.5 KCl, 1.25 NaH_2PO_4, 30 $NaHCO_3$, 20
550 HEPES, 25 glucose, 2 thiourea, 5 Na-ascorbate, 3 Na-pyruvate, 2 $CaCl_2$, 2 $MgSO_4$). Slices
551 recovered for an additional 60 min.

552

553 **Slice electrophysiology:** Whole-cell patch-clamp recordings were made using an Axopatch
554 700B amplifier (Molecular Devices) with sampling at 10 kHz and filtering at 1 kHz. eYFP+ cells
555 were visually identified via fluorescence for patching with electrodes at 3–5 MΩ. Series
556 resistance was monitored during all recordings with changes in resistance ± 20% qualifying the
557 cell for exclusion. Recordings were made in aCSF (in mM: 126 NaCl, 2.5 KCl, 1.2 NaH_2PO_4,
558 1.2 $MgCl_2$ 11 D-glucose, 18 $NaHCO_3$, 2.4 $CaCl_2$) at 32°C continually perfused over slices at a
559 rate of ~2 ml/min. VTA dopamine neurons were identified by fluorescence. Electrodes were
560 filled with an internal solution containing (in mM): 130 potassium gluconate, 10 HEPES, 5
561 NaCl, 1 EGTA), 5 Mg2+/ATP, 0.5 Na+-GTP, pH 7.3, 280 mOsmol.

562

563 **Spontaneous activity, excitability, and action potential shape measurements:** Spontaneous
564 activity was recording in I=0 mode for 1 minute and I/V curves (0-80 pA, 10 pA steps, 1 s) for
565 excitability were immediately measured in I-Clamp mode (done both at cell's resting membrane
566 potential in fig. S4, O and when holding the cell at -60 mV in Fig 2, G-H). All data were
567 analyzed offline using Clampfit (Molecular Devices). Frequency of spontaneous activity was
568 calculated as number of events/s and CV-ISI was measured using the standard deviation of the
569 interspike interval (ISI) from spontaneous activity. Excitability was measured as the total number
570 of events during each current step. Action potentials of spontaneous activity were detected using
571 the Event Detection function in Clampfit (restricted window parameters: between 50 ms before
572 action potential peak and 150 ms after action potential peak) and used to determine firing
573 frequency and CV-ISI, and action potential shape analysis from baseline resting membrane
574 potential. For action potential shape analysis in a clamped cell, the first action potential of

575 activity elicited from a 20 pA current injection while the cell was being held at -60 mV was
576 detected using the Event Detection function in Clampfit with identical restricted window
577 parameters. Event statistics from the Event Detection function were extracted, including action
578 potential peak, half-width, decay tau, and afterhyperpolarization (the anti-peak Event Statistics
579 characteristic corrected for resting membrane potential measure 50 ms before spike peak). For
580 each cell, detected action potentials were averaged to visualize action potential waveforms and
581 phase plane plots. Phase plane plots were calculated as the dV/dt and plotted as the dV/dt over
582 voltage. Action potential threshold was defined as the point at which dV/dt of the AP waveform
583 reaches 4% of its maximum (*23*). Resting membrane potential was recorded as the membrane
584 potential at the beginning of the action potential waveform from the Event Detection window (50
585 ms before peak). For action potential shape analysis of control VTA dopamine neurons following
586 pharmacological inhibition of A-Type or BK potassium currents, AmmTx3 (10 nM, Tocris) and
587 Iberiotoxin, (150 nM, Cayman Chemical) were perfused onto the slice in oxygenated aCSF and
588 spontaneous activity was recorded. Shape analyses were performed as described above.
589
590 **Potassium current measurements:** For A-Type and BK potassium channel current, I_A and I_{BK}
591 respectively, recordings in V-Clamp mode, aCSF was supplemented with 500 nM TTX to
592 eliminate action potential activity and cells were held at -60 mV. I_A was activated using voltage
593 steps from -108mV to -28 mV to -48mV then back to holding potential every 5 s, 5 times.
594 AmmTx3 (10 nM, Tocris) was used to pharmacologically block Kv4 channels. I_{BK} was measured
595 using subtraction before and after pharmacological inhibition of BK channels (iberiotoxin, 150
596 nM (Cayman Chemical)) during depolarizing voltage steps that activated I_K from -63mV to
597 +2mV to -48 mV to -63 mV every 5 s, 5 times. Data were analyzed offline using Clampfit. For

598 A-type potassium currents, differences between the peaks at the -28mV and the -48 mV step
599 were determined and calculated. For quantifying BK currents, we first present in Fig. 1, J-K
600 maximal peaks of raw I_K in Fig. 1, J-K before (-, I_K^{Pre}) and after (+, I_K^{Post}) application of the BK
601 channel specific inhibitor iberiotoxin from mice that received control virus or sgKcnma1 virus to
602 knockdown *Kcnma1* (BKCa1.1). A significant difference from I_K^{Pre} either indicates an
603 iberiotoxin specific effect indicative of BK channel blockade or a CRISPR/cas9 LOF effect
604 indicative of BKCa1.1 knockdown. Notably, no difference between sgKcnma1 I_K^{Pre} and I_K^{Post}
605 indicates that there is no iberiotoxin-sensitive current (I_{BK}). We also present the subtracted I_{BK} in
606 fig. S4, A-C. which was calculated by subtracting I_K^{Post} from I_K^{Pre}. We then measured the
607 maximal peak generated from the depolarization and the total area under the curve to quantify
608 I_{BK} .
609
610 ***In vivo* single-unit electrophysiology:** Recordings began at least 4 weeks after surgery in a
611 recording cage with corncob bedding or during behavior using Neuralynx acquisition hardware
612 and software (Digital Lynx 4SX, Cheetah Data Acquisition). For *in vivo* electrophysiology
613 recordings during behavior (behaviors described below), mice were recorded in operant
614 chambers (MedAssociates) that were interfaced with the Data Acquisition software. For all
615 experiments, the ceramic ferrule of the optic fiber in the microdrive was attached to a patch cord
616 that was connected to a 473 nm blue laser (Laserglow technologies). A preamplifier was
617 connected to the microdrive's EIB. Recordings were acquired either in the home cage or during
618 behavior through Cheetah Data Acquisition. Optical stimulations were synced through Cheetah
619 with a function generator (Agilent). Data were continuously sampled, amplified, and filtered
620 between 100 and 9000 Hz, and digitized at 32 kHz. If the spike exceeded a predetermined

621 threshold, discretely sampled data were recorded and filtered between 100 and 6000 Hz. At the
622 end of the recording, 10 blue light pulses were delivered 20 times through the optic fiber of the
623 microdrive to activate neurons that expressed ChR2 (5 ms long at 20 Hz, putative dopamine
624 neurons). The light intensity (5-15 mW/mm2) was adjusted so that light-evoked spike
625 waveforms were similar to spontaneous ones. This was followed by quinpirole injections
626 (described below). All optetrodes were lowered in 80 µm increments at the end of the day to
627 identify a new cell field the next day. Data were analyzed offline using Plexon Offline Sorter,
628 SpikeSort3D, Neuroexplorer, and Matlab, as previously described (*30*). Briefly, units were
629 identified using cluster analysis in the Offline Sorter or SpikeSort3D (KlustaKwik) and saved.
630 Frequency, burst analysis, and blue-light sensitive (ChR2 expressing putative dopamine neurons)
631 identification were performed in Neuroexplorer and Matlab. Putative dopamine neurons were
632 identified as either sensitive to ChR2 stimulation or sensitive to pharmacological identification:
633 light/optically sensitive putative dopamine neurons were identified as those that had a spike
634 latency of $\leq$5 s and 0.6 probability during blue light activation of ChR2; pharmacologically-
635 sensitive putative dopamine neurons were identified as those that had a reduction in firing rate to
636 30% or less of baseline after an i.p. injection of 0.2 mg/kg of quinpirole chloride (example
637 histogram in fig. S5, C), a dopamine receptor D2 agonist expressed on a significant
638 subpopulation of dopamine neurons *(11)*. The onset of a burst was identified as two consecutive
639 spikes with an inter-spike interval of <80 ms and its termination was defined as an inter-spike
640 interval of >160 ms (*30*).

641 The latency to spike and probability of spiking after ChR2 stimulation under baseline and
642 behavioral conditions are reported in fig. S5, C. Optically-sensitive putative dopamine units from
643 mice that underwent recordings only in the home cage and optically-sensitive putative dopamine

644 units that were recorded during operant conditioning that were not responsive to a lever press
645 (LP) during behavior were included in the analysis of baseline firing properties reported in Fig.
646 2, L-M and fig. S5, D-F. Cells that were identified to be responsive to LP events were not
647 included in analysis of baseline properties due to potential confounds of peri-event activity but
648 their mean firing rates are reported in fig. S7 and S10. For analysis of *in vivo* firing of putative
649 dopamine neurons during a LP, 20 s window (± 10 s) peri-event windows surrounding the LP
650 during FR1 reinforced day 1 and day 5, and extinction day 1 were extracted and z-scores
651 calculated using the first 3 s (-10 to -7 s) of the peri-event window as the peri-event baseline. To
652 determine which units were behaviorally responsive to the LP, optically- and pharmacologically-
653 sensitive units that had a ± 3 STDs shift from the median baseline (-10 to -7 s prior to LP) within
654 ± 1 s of the LP event were extracted. AUCs were then determined for these events: LP (0 to 0.7 s
655 post LP) and Rew (3 s post LP to 6 s post LP).
656
657 **Overnight locomotor activity:** 4 weeks after surgery, baseline locomotion was measured using
658 locomotion chambers (Columbus instruments) that use infrared beam breaks to calculate
659 ambulatory activity. Mice were singly housed and provided with *ad libitum* access to food and
660 water. Locomotion was monitored for 60 consecutive hours (Friday-Monday: 3 nights, 2 days).
661 Behavioral tracking failed for one BKCa1.1LOF mouse, however this mouse was still included
662 in operant studies.
663
664 **Open field test:** At least 4 weeks after surgery, mice were tested on an open field test to
665 determine alterations in exploration and anxiety. Here, mice we placed into a large circular arena
666 (120 cm diameter) and activity was recorded for a period of 10 min. behavior was analyzed

667 offline using Ethovision software (Noldus). Here, zones arena edge and arena center zones were
668 generated. Time in center (a marker of exploratory/anxiolytic behavior) and total distance were
669 calculated.
670
671 **Elevated plus maze test:** At least 4 weeks after surgery, mice were tested on an elevated plus
672 maze (Med Associates) to determine alterations in anxiety. The plus-shaped maze has two
673 opposing closed-walled arms and two opposing open-ledge (1 cm tall) arms with a center zone.
674 The floors of the maze are white. A mouse was placed into the center zone and allowed to freely
675 explore the maze for 10 min. Video was recorded and analyzed offline using Ethovision. Total
676 distance traveled and time spent in the center, closed, and open arms were determined. Percent
677 time spent in arms was calculated (a marker of anxiolytic behavior).
678
679 **Pavlovian conditioning:** At least 4 weeks after surgery, mice were food restricted to 85% of
680 their body weight and were maintained at this bodyweight for all conditioning days.
681 Conditioning sessions took place in mouse conditioning boxes outfitted with a house light,
682 ultrasensitive levers, a food hopper with a head entry detector, nose poke holes, and barred floors
683 (MedAssociates). Pavlovian training sessions consisted of 25 trials in which 10 s lever extension
684 (an audiovisual CS). After 10 s lever presentation, levers were retracted and a sucrose pellet
685 reward (Rew, 20 mg sucrose pellet, Bioserv) was delivered in the food hopper. Each trial was
686 separated by a random inter-trial interval averaging 70 s and animals underwent 7 days of
687 training. The house light remained on during the entire session. Conditioned approach scores
688 were calculated as the rate of head entries during the CS - rate of head entries during the ITI.
689 Mice used for *in vivo* electrophysiology or dLight experiments first underwent 3 days of 20 min

690 acclimation sessions to patch cord tethering in the conditioning boxes followed by 10 days of
691 Pavlovian conditioning while tethered.
692
693 **Operant conditioning:** After Pavlovian conditioning, mice began an FR1 schedule of reinforced
694 operant conditioning. Each session lasted for 60 min. Here, levers were extended and remained
695 extended until a LP. Upon a lever press, levers were retracted, and a sucrose pellet was
696 immediately delivered into the food hopper (Rew). For *in vivo* electrophysiology or dLight
697 experiments during FR1 reinforced training, a temporal delay of 3 s between LP and Rew was
698 included to dissociate dynamics of LP and Rew. The levers did not extend again until the mouse
699 entered the food hopper to retrieve the sucrose pellet. The house light remained on during the
700 entire session. Reinforced FR1 sessions lasted for 3 days (5 days for tethered mice). A subset of
701 mice then underwent a progressive ratio test where the number of lever presses necessary for
702 sucrose pellet delivery increases non-arithmetically (i.e., 1, 2, 4, 6, 9, 13…) over the course of
703 the session. The progressive ratio session automatically ended after 3 consecutive min of no
704 lever presses or after 3 hours. Another subset of mice that had undergone FR1 reinforced training
705 underwent FR1 extinction for 60 min each session for five days. Here, levers extend and retract
706 similarly to the FR1 reinforced paradigm, yet a sucrose pellet reward is omitted after a LP. Mice
707 underwent extinction for 5 days. *In vivo* electrophysiology and dLight mice also underwent 5
708 days of extinction training following completion of FR1 reinforced training.
709
710 **dLight recordings using fiber photometry during operant conditioning:** Fiber photometry
711 recordings lasted the entirety of the behavioral conditioning sessions (first and last days of
712 reinforced FR1 and extinction FR1). dLight1.3b was used to measure dopamine release in the

713 NAc during these behaviors of control or CRISPR mice. Prior to every session, the implanted
714 optic fiber was attached to a previously photobleached patchcord (Doric Lenses) using a ceramic
715 sleeve (Doric Lenses). Recordings were acquired using an RZ5 BioAmp Processor from Tucker
716 Davis Technologies (TDT). A 465 nm LED (531-Hz, sinusoidal, Doric Lenses) was used to
717 excite dLight1.3b and a 405 nm LED was used as an isosbestic control (211-Hz, sinusoidal,
718 Doric Lenses) using an LED driver (Doric Lenses) controlled via the RZ5. Prior to each session,
719 patch cords had been photobleached for at least one hour. Laser intensities were measured at the
720 tip of the optic fiber to reach levels of 30-45 uW before being bandpass filtered (525 ± 25 nm,
721 Doric, FMC4), transduced by a femtowatt silicon photoreceiver (Doric Lenses), and recorded by
722 a real-time processor (TDT, RZ5). The 531-Hz and 211-Hz signals were extracted in real-time
723 by the TDT program Synapse at a sampling rate of 1017.25 Hz. MedAssociate signals of
724 behavioral events such as LP and Rew were synced to the recordings for further analysis offline.
725
726 **Photometry analysis of perievents:** A custom software GUI was generated to extract,
727 downsample and z-score the photometry signals surrounding behavioral events for each mouse
728 (20 s window: ± 10 s behavioral event). Data were first downsampled to 100 Hz and DF/F was
729 calculated using the custom software GUI. Next, Z-score was calculated relative to the mean and
730 standard deviation of the first 4 s of the 20 s time window (baseline perievent time). Mouse data
731 were further processed in custom MatLab script. Z-scores for each mouse were then
732 downsampled to 50 Hz and then averaged. Data were exported to GraphPad Prism for statistical
733 analysis, area under the curve (AUC) analysis, peak analysis and trace export. For reinforced
734 FR1 training and omission extinction training, AUC time bins were calculated for a set time
735 following the event: LP (3 s post), Rew (5 s post).

736

737 **Two(2)-photon slice imaging of dLight:** NAc slices were transferred to a heated recording in
738 aCSF (in mM: 126 NaCl, 2.5 KCl, 1.2 NaH_2PO_4, 1.2 $MgCl_2$ 11 D-glucose, 18 $NaHCO_3$, 2.4
739 $CaCl_2$) at 32°C continually perfused over slices at a rate of ~2 ml/min on an Olympus Fluoview
740 FVMPE-RS 2-photon microscope. The NAc was identified using anatomical markers and
741 epifluorescence and expression of dLight GFP and VTA dopamine terminals expressing
742 Chrimson-TdTomato was quickly confirmed before recording. Previous reports have found that
743 this preparation does not induce stimulation of Chrimson (*36*). We used a resonant scanner (30
744 Hz frame rate acquisition) and performed an online averaging of 6 times to get an effective frame
745 rate of 5 Hz. A GaAsP-PMT with adjustable voltage, gain and offset was used, along with a
746 green filter cube. We used a 25x immersion objective (Olympus, XLPLN25XWMP, 1.05 NA, 2
747 mm WD) and imaged with a 920 nm laser (SpectraPhysics, ~100 fs pulse width) with automated
748 wavelength-specific alignment. Chrimson fibers in the NAc were stimulated at increasing
749 frequencies for 1 s following a 10 s baseline using full field 615 nm LED stimulation through the
750 objective (CoolLED, PE-100). Data were analyzed in FiJi ImageJ using the Time Series
751 Analyzer plug in. Z-score of fluorescence was calculated from a 10 s baseline preceding the
752 Chrimson stimulation. AUC calculations were performed in GraphPad Prism.

753

754 **Statistics:** Data were analyzed for statistical significance using GraphPad Prism. Data
755 distribution was assumed to be normal but this was not formally tested. No statistical methods
756 were used to predetermine sample sizes, but our sample sizes are similar to those reported in
757 previous publications (*11-13, 30*). Littermates were randomly assigned to experimental groups and
758 animals were tested in a random order across all biological replicates. All behavioral assays were

759 repeated in a minimum of three cohorts with similar replication of results. Data for *in situ*
760 hybridization, genetic validation of mutagenesis, 2-photon imaging, and fiber photometry were
761 pooled from at least three individual animals, collected from at least two rounds of experiments
762 with similar replication of results. VTAs for qPCR were pooled from at least two mice per group.
763 Electrophysiology data are from individual cells collected from at least two individual animals
764 and collected from at least two rounds of experiments with similar replication of results. Data
765 were analyzed by an investigator blinded to experimental condition; the experimenter was not
766 blinded during data collection. Animals with missed viral injections or significant viral spread
767 outside the targeted region were excluded from analyses. These criteria and other
768 inclusion/exclusion criteria described above were preestablished. All statistical tests were two-
769 sided, except for ratio data in fig. S9, G and correlational data in fig. S9, H, and when
770 appropriate corrected for multiple comparisons to controls (Fisher's or Dunnet's), except for
771 current data in Fig. 1 G and K where a Sidak's test was used for pharmacological blockade
772 analysis. Detailed statistical analyses can be found in the figure legends.
773
774

775 **Acknowledgments**
776 We would like to thank members of the Zweifel, Palmiter, and Chavkin laboratories at
777 the University of Washington for their helpful discussions. We would also like to thank the staff
778 of the University of Washington's Molecular Genetics Research Core, Imaging and Neural
779 Circuits Core, Comparative Medicine Animal Facilities, the University of Washington's Keck
780 Imaging Center, and the University of Washington's Pathology Flow Cytometry Core.

781 **Funding:**
782 This study was supported by:

783 K99-DA054265 (B.J.)

784 R00-DA054265 (B.J.)

785 T32-DA727825 (B.J.)

786 F32 MH127801 (M-S.K)

787 F31 DA053724 (J.E.E)

788 F31-MH116549 (A.C.H.)

789 T32-GM007270 (A.C.H.)

790 F31 MH126489 (M.C.)

791 T32-GM007270 (M.C.)

792 R03TR003307 (M.E.S.)

793 R01-MH104450 (L.S.Z.)

794 R01-DA044315 (L.S.Z.)

795 University of Washington's Addictions, Drugs and Alcohol Institute:

796 ADAI-1019-17 (B.J.)

797 National Research Foundation of Korea:

798 MEST 2020R1A2C2102134 (Y.S.J)

Core grants:

S10OD016240 (University of Washington Keck Center)

P30-DA048736 (University of Washington Center of Excellence in Opioid Addiction Research)

B.J. was funded by the postdoctoral Enrichment Program Award from the Burroughs Wellcome Fund.

Author contributions:

Conceptualization: BJ, LSZ
Methodology: BJ, MES, SN-E, LSZ
Investigation and analysis: BJ, M-SK, YSJ, JEE, JXY, MC, ACH, MAQ, MAB, MJ, DB AM, NLG, LSZ
Visualization: BJ, ACH, LSZ
Supervision: BJ, LSZ
Writing—original draft: BJ, LSZ
Writing—review & editing: all authors reviewed and approved this manuscript. BJ and LSZ edited the manuscript following co-author review.

Competing interests: All other authors declare they have no competing interests.

Data and materials availability: Data, materials, and code can be made available upon request.

822 **Figure legends:**

823

824 **Fig. 1 Targeted mutagenesis of *Kcnd3* and *Kcnma1* in dopamine neurons.**

825 (**A-B**) RNAscope *in situ* hybridization for *Kcnd3*, *Kcnma1*, and *Th*. White arrows: representative
826 *Th/Kcnd3/Kcnma1* overlap. Scale bar, 100 µm (**A**) and 50 µm (**B**). (**C**) Quantification of overlap
827 for *Kcnd3, Kcnma1,* and *Th* in the VTA (N=3 mice). (**D**) Schematic of AAV1-FLEX-SaCas9-
828 sgKcnd3 targeting virus vector. (**E**) Proportion of targeted deep sequencing reads with indel
829 mutations following sgKcnd3 targeting (N=5 mice). (**F**) Average pre- and post-AmmTx A-Type
830 currents (I_A) from control (left) and sgKcnd3 (right) -targeted mice (N=4 cells/group; 3
831 mice/group) and corresponding depolarization step to elicit I_A. (**G**) Average peak I_A from (**F**) in
832 control and sgKcnd3-targeted mice (Two-way RM ANOVA, Interaction effect $F_{(1,6)}$=18.96,
833 P<0.01; Group effect $F_{(1,6)}$=22.6, P<0.01; Drug effect $F_{(1,6)}$=16.1, P<0.01; Sidak's Multiple
834 Comparison test, ***p<0.001; $N_{control}$=4 cells, 3 mice, $N_{sgKcnd3}$=4 cells, 3 mice). (**H**) Schematic of
835 AAV1-FLEX-SaCas9-sgKcnma1 targeting virus vector. (**I**) Proportion of targeted deep
836 sequencing reads with indel mutations following sgKcnma1 targeting (N=5 mice). (**J**) Average
837 pre- and post-iberiotoxin potassium currents (I_K) from control (left) and sgKcnma1 (right) -
838 targeted mice ($N_{control}$=11 cells, 4 mice; $N_{sgKcnma1}$=11 cells, 3 mice) and corresponding
839 depolarization step to elicit I_K. (**K**) Peak I_K from (**J**) in control and sgKcnma1-targeted mice before
840 (-) and after (+) iberiotoxin (Two-way RM ANOVA, Interaction effect $F_{(1,19)}$=18.45, P<0.001;
841 Group effect $F_{(1,19)}$=6.553, P<0.05; Drug effect $F_{(1,19)}$=69.84, P<0.0001; Sidak's Multiple
842 Comparison test, *p<0.05, ***p<0.001; $N_{control}$=11 cells, 4 mice; $N_{sgKcnma1}$=11 cells, 3 mice). Box
843 and whisker graphs are presented as min-to-max.

844

845 **Fig. 2 Kv4.3 and BKCa1.1 LOF alter the dopamine action potential waveform and activity.**
846 (**A**) Average action potential waveform from spontaneously active VTA dopamine neurons
847 ($N_{control}$=21 cells, 7 mice, $N_{Kv4.3LOF}$=16 cells, 6 mice, $N_{BKCa1.1}$=19 cells, 7 mice). (**B**) Representative
848 phase plane plot of action potential dynamics. (**C**) Action potential half width in control, Kv4.3
849 LOF, and BKCa1.1 LOF cells (One-Way ANOVA: $F_{(2,53)}$=9.109, P<0.001, Dunnet's Multiple
850 Comparison's test to controls,t ***p<0.001). (**D**) Decay kinetics of the action potential (One-Way
851 ANOVA: $F_{(2,53)}$=10.67, P<0.0001, Dunnet's Multiple Comparison's test to controls, ***p<0.001).
852 (**E**) Afterhyperpolarization of the action potential (One-Way ANOVA: $F_{(2,53)}$=5.314, P<0.01,
853 Dunnet's Multiple Comparison's test to controls, *p<0.05). (**F**) Resting membrane potential (One-
854 Way ANOVA: $F_{(2,53)}$=6.026, P<0.01, Dunnet's Multiple Comparison's test to controls, **p<0.01).
855 (**G**) Representative evoked excitability traces. (**H**) Current-voltage plot (Two-Way ANOVA,
856 Interaction effect: $F_{(16, 408)}$ = 1.143, P=0.3126; Group effect: $F_{(2, 51)}$ =4.495 P<0.05; Current effect:
857 $F_{(8, 408)}$ =69.36 P<0.0001; Dunnet's Multiple Comparison's test to controls: *p<0.05, **p<0.01;
858 $N_{control}$=19 cells, $N_{Kv4.3\ LOF}$=15 cells, $N_{BKCa1.1LOF}$=20 cells). (**I**) Representative spontaneous activity
859 traces. (**J**) Firing rate of spontaneous activity (One-Way ANOVA: $F_{(2,53)}$=3.379, P<0.05, Dunnet's
860 Multiple Comparison's test to controls, *p<0.05). (**K**) CV-ISI of spontaneous activity (One-Way
861 ANOVA: $F_{(2,53)}$=3.606, P<0.05, Dunnet's Multiple Comparison's test to controls, *p<0.05). (**C-F**
862 and **J-K**; $N_{control}$=21 cells, 7 mice, $N_{Kv4.3LOF}$=16 cells, 6 mice, $N_{BKCa1.1}$=19 cells, 7 mice). (**L**) Burst
863 rate in VTA dopamine neurons *in vivo* (One-Way ANOVA: $F_{(2,117)}$=5.673, P<0.01, Dunnet's
864 Multiple Comparison's test to controls **p<0.001). (**M**) Burst duration in VTA dopamine neurons
865 *in vivo* (One-Way ANOVA: $F_{(2,117)}$=5.366, P<0.01, Dunnet's Multiple Comparison's test to
866 controls, *p<0.05). (**L-M** $N_{control}$=28 cells, 7 mice, $N_{Kv4.3\ LOF}$=49 cells, 10 mice, and $N_{BKCa1.1}$=41
867 cells, 9 mice). (**N**) Schematic of 2-photon slice imaging of dLight1.3b with optically evoked

868 dopamine release of VTA terminals expressing Chrimson + sgRNA in the NAc. (**O**) Average
869 dLight1.3b signal following 1 s stimulation at different frequencies in control, Kv4.3 LOF and
870 BKCa1.1 LOF mice. (**P**) Average AUC for responses for data presented in panel **O** (Mixed effects
871 analysis, Interaction effect $F_{(6, 77)}$=0.6984, P=0.6516, Group effect $F_{(2, 26)}$=0.05105, P=0.9503,
872 Frequency stimulation effect $F_{(1.725, 44.28)}$=25.99, P<0.0001). (**P-O**, $N_{control}$=6 slices, 5 mice;
873 $N_{Kv4.3LOF}$=8 slices, 4 mice; $N_{BKCa1.1LOF}$=15 slices, 3 mice; except for 5 Hz where $N_{Kv4.3LOF}$=7 slices
874 because of brief interruption in data capture that was not detected until post-hoc analysis,). Trace
875 averages are presented as mean + SEM. Box and whisker graphs are presented as min-to-max.
876

877 **Fig. 3 Pavlovian and instrumental behavior in control, Kv4.3, and BKCa1.1 LOF mice.**

878 (**A**) Schematic of Pavlovian conditioning paradigm. (**B**) Conditioned approach score (head entries
879 during CS+ - head entries during ITI) across days is not different between groups, (Two-Way RM
880 ANOVA, Interaction effect: $F_{(12, 378)}$=1.557, P=0.1019; Time effect: $F_{(5, 378)}$=31.97, P<0.0001;
881 Group effect: $F_{(2, 63)}$=1.093, P=0.3416) (**C-D**) Head entry rate during CS (C) and ITI period (D)
882 across days used to calculate conditioned approach is not different between groups, (Two-Way
883 RM ANOVA Control ITI vs Cue comparison: Interaction effect $F_{(6, 276)}$=3.86, P<0.01; Time effect
884 $F_{(3.403, 156.5)}$=249, P<0.0001; ITI vs Cue effect $F_{(1, 46)}$=6.433, P<0.05; Kv4.3 LOF ITI vs Cue
885 comparison: Interaction effect $F_{(6, 288)}$=2.555, P<0.05; Time effect $F_{(3.403, 156.5)}$=249, P<0.0001; ITI
886 vs Cue effect $F_{(1, 46)}$=6.433, P<0.05; BKCa1.1 LOF ITI vs Cue comparison: Interaction effect $F_{(6,}$
887 $_{204)}$=4.286, P<0.0001; Time effect $F_{(4.053, 137.8)}$=36.36, P<0.0001; ITI vs Cue effect $F_{(1, 34)}$=6.989,
888 P<0.05; Sidak's Multiple Comparison's test, Cue vs ITI, *p<0.05). (**B-D** $N_{control}$=23; $N_{Kv4.3LOF}$=25;
889 $N_{BKCa1.1LOF}$=18). (**E**) Schematic of instrumental FR1 conditioning paradigm. (**F**) Lever presses
890 during days 1-3 of FR1 conditioning (Two-Way RM ANOVA Interaction effect $F_{(4, 106)}$=2.781,
891 P<0.05; Time effect $F_{(1.631, 86.42)}$=18.26, P<0.0001; Group effect $F_{(2, 53)}$=0.9557, P=0.3911; Subject
892 effect $F_{(53, 106)}$=2.018, P<0.01; Dunnet's Multiple Comparison's test to controls, *p<0.05). (**G**)
893 Cumulative lever presses during day 1 (left) and day 3 (right) of FR1 conditioning (Two-Way RM
894 ANOVA, Day 1: Interaction effect $F_{(118, 3127)}$=3.769, ****P<0.0001; Time effect $F_{(1.807,}$
895 $_{95.78)}$=143.0, P<0.0001; Group effect $F_{(2, 53)}$=4.832, P<0.05; Subject effect $F_{(53, 3127)}$=167.2,
896 P<0.0001; Dunnet's Multiple Comparison's test to controls, Control vs BKCa1.1LOF: p<0.05 for
897 mins 35-42; p<0.01 for mins 43-60; Day 3: Interaction effect $F_{(118, 3127)}$=1.455, **P<0.01; Time
898 effect $F_{(1.288, 68.26)}$=228.8, P<0.0001; Group effect $F_{(2, 53)}$=4.299, P<0.05; Subject effect $F_{(53,}$
899 $_{3127)}$=152.3, P<0.0001; Dunnet's Multiple Comparison's test to controls, Control vs Kv4.3 LOF:

900 $p<0.05$ for mins 2, 6-26; $p<0.01$ for mins 3-5;). (**H**) Lever press ethograms during day 1 of FR1
901 conditioning. (**I**) Frequency distribution of lever inter-press intervals during the first and second
902 half of the conditioning session for day 1 (Two-Way RM ANOVA, first half: Interaction effect
903 $F_{(72, 1908)}=2.706$, ****$P<0.0001$; Time effect $F_{(2.888, 153.1)}=20.67$, $P<0.0001$; Group effect $F_{(2,}$
904 $_{53)}=3.458$, $P<0.05$; Subject effect $F_{(53, 1908)}=3.834$; Dunnet's Multiple Comparison's test to controls,
905 30 s: $p<0.05$ for control vs Kv4.3 LOF; second half: Interaction effect $F_{(72, 1908)}=1.012$, $P=0.4510$;
906 Time effect $F_{(4.049, 214.6)}=21.56$, $P<0.0001$; Group effect $F_{(2, 53)}=1.529$, $P<0.2263$; Subject effect
907 $F_{(53, 1908)}=2.389$, $P<0.0001$). (**J**) Lever press ethograms during day 3 of FR1 conditioning. (**K**)
908 Frequency distribution of lever inter-press intervals during the first and second half of the
909 conditioning session for day 3 day 3 (Two-Way RM ANOVA, first half: Interaction effect $F_{(72,}$
910 $_{1908)}=1.923$, $P<0.0001$; Time effect $F_{(3.798, 201.3)}=29.10$, $P<0.0001$; Group effect $F_{(2, 53)}=4.482$,
911 $P<0.05$; Subject effect $F_{(53, 1908)}=1.470$, $P<0.05$, Dunnet's Multiple Comparison's test to controls,
912 20 s: p<.0.05 Kv4.3LOF vs BKCa1.1LOF; 25 s: $p<0.01$ for Kv4.3LOF vs BKCa1.1LOF; 125 s:
913 $p<0.05$ control vs Kv4.3LOF; Second half: Interaction effect $F_{(72, 1908)}=1.037$, $P=0.3950$; Time
914 effect $F_{(2.581, 136.8)}=19.91$, $P<0.0001$; Group effect $F_{(2, 53)}=0.6340$, $P<0.5344$; Subject effect $F_{(53,}$
915 $_{1908)}=3.668$, $P<0.0001$). (**F-I:** $N_{control}=19$; $N_{Kv4.3LOF}=24$; $N_{BKCa1.1LOF}=13$). **B-D** and **F** data are
916 presented as mean ± SEM. Cumulative lever press trace data presented as mean ± SEM and IPI
917 data presented as mean + SEM.
918

919 **Figure 4 Differential action potential firing in putative dopamine neurons from control,**
920 **Kv4.3 LOF, and BKCa1.1 LOF mice during instrumental conditioning.** (**A**) Schematic of
921 instrumental conditioning paradigm. (**B**) Illustration of optetrode Microdrive placement in the
922 VTA and injections of AAV1-FLEX-ChR2-eYFP + AAV1-FLEX-SaCas9-sgRNA injection in
923 DAT-IRES-Cre mice. (**C**) Average peri-event Z-score for putative dopamine neurons responsive
924 to LP in the VTA for day 1 (top row) and day 5 (middle row and bottom row) (day 1: $N_{control}$=17
925 cells, 2 mice; $N_{Kv4.3LOF}$=39 cells, 5 mice; and $N_{BKCa1.1LOF}$=13 cells, 3 mice; day 5: $N_{control}$=8 cells,
926 3 mice; $N_{Kv4.3LOF}$=16 cells, 3 mice; and $N_{BKCa1.1LOF}$=15 cells, 3 mice). (**D**) Average area under the
927 curve (AUC) for the peri-event Z-score action potential firing post-LP period on day 1 (One-way
928 ANOVA, $F_{(2,66)}$= 6.29, P=0.0031, Fischer's direct comparison to controls, **p<0.01; $N_{control}$=17, 2
929 mice; $N_{Kv4.3LOF}$=39 cell, 5 mice; $N_{BKCa1.1LOF}$=13 cells, 3 mice) and day 5 (One-way ANOVA,
930 $F_{(2,44)}$= 25.56, P<0.001, Fisher's direct comparison to controls, **p<0.05, $N_{control}$=8 cells, 2 mice;
931 $N_{Kv4.3LOF}$=16 cells, 3 mice; $N_{BKCa1.1LOF}$=15 cells, 3 mice). (**E**) Average AUC for the Z-score of
932 action potential firing for post-Rew period on day 1 and day 5 (day 1, One-way ANOVA, $F_{(2,66)}$=
933 4.07, P=0.022; Day 1: $N_{control}$=17 cells, 2 mice; $N_{Kv4.3LOF}$=39 cells, 5 mice; $N_{BKCa1.1LOF}$=13 cells, 3
934 mice; day 5: One-way ANOVA, $F_{(2,44)}$=3.875, P=0.028, Fischer's direct comparison to controls,
935 **p<0.01; $N_{control}$=8 cells, 3 mice; $N_{Kv4.3LOF}$=16 cells, 3 mice; $N_{BKCa1.1LOF}$=15 cells, 3 mice).
936 Averaged traces are presented as mean + SEM. Box and whisker graphs are presented as min-to-
937 max.

938

939 **Figure 5 Differential dopamine dynamics in the NAc of control, Kv4.3 LOF, and BKCa1.1**
940 **LOF mice during instrumental conditioning.** (**A**) Average peri-event Z-score for dLight1.3b
941 signals in the NAc for day 1 (top row) and day 5 (middle row and bottom row). (**B**) Average AUC
942 for the perievent Z-score dLight1.3b signals post-LP period (3 s) (day 1, one-way ANOVA $F_{(2, 14)}$
943 =4.456, P<0.05; day 5, one-way ANOVA $F_{(2, 14)}$=2.867, P=0.09, Fisher's direct comparison to
944 controls, *p<0.05). (**C**) Average AUC for the perievent Z-score dLight1.3b signals post-Rew
945 period (day 1, one-way ANOVA $F_{(2, 14)}$ =6.701, P<0.01; day 5, one-way ANOVA $F_{(2, 14)}$=2.468,
946 P=0.12, Fisher's direct comparison to controls, *p<0.05). (**D**) Zoomed average peri-event Z-score
947 on day 5 for dLight1.3b in the NAc from panel A showing ramping in the pre-LP period. (**E**)
948 Average ramp to peak Z-score from dLight1.3b signals in the NAc for pre-LP period (One-way
949 ANOVA, $F_{(2,14)}$=3.848, p<0.05, Fisher's direct comparisons to controls *p<0.05). (**A-E**: $N_{control}$=6
950 mice; $N_{Kv4.3LOF}$=6 mice; $N_{BKCa1.1LOF}$=5 mice). Averaged traces are presented as mean + SEM. Box
951 and whisker graphs are presented as min-to-max.

952

953

954

955

956

957 **Figure 6 Extinction behavior and dopamine signal diametrically changes in Kv4.3 and**
958 **BKCa1.1 LOF mice.**

959 (**A**) Schematic of instrumental FR1 extinction paradigm. (**B**) Lever presses during days 1-5 of
960 extinction training (Two-way RM ANOVA, Interaction effect $F_{(8, 136)}$=7.35, P<0.0001; Time effect
961 $F_{(4, 136)}$=90.43, P<0.0001; Group effect $F_{(2, 34)}$=6.30, P=0.0047; Subject effect $F_{(34, 136)}$=2.911,
962 P<0.0001; Dunnet's Multiple comparison's test to controls, ***p<0.001, ****p<0.0001, vs.
963 control). (**C**) Frequency distribution of lever presses during the first and second half of the
964 conditioning session for day 1 of extinction (Two-way RM ANOVA, <u>first half:</u> Interaction effect
965 $F_{(72, 1152)}$=10.31, ****P<0.0001; Time effect $F_{(1.141, 36.51)}$=57.07, P<0.0001; Group effect $F_{(2,}$
966 $_{32)}$=12.42, P<0.0001; Dunnet's multiple comparison's test to controls, 5 s: p<0.01 for control vs
967 Kv4.3LOF; 45 s: p<0.05 for control vs BKCa1.1LOF; <u>second half:</u> Interaction effect $F_{(72,}$
968 $_{1152)}$=5.047, P<0.0001; Time effect $F_{(1.459, 46.60)}$=48.96, P<0.0001; Group effect $F_{(2, 32)}$=5.851,
969 P<0.01, Dunnet's multiple comparison's test to controls, 5 s: p<0.05 for control vs Kv4.3LOF).
970 (**B-C**, $N_{control}$=13, $N_{Kv4.3LOF}$=10, and $N_{BKCa1.1LOF}$=12;) (**D**) Average Z-score for putative dopamine
971 neurons in the VTA during FR1 day 1 following LP (top) compared to average Z-score following
972 LP on day 1 of extinction (FR1 day 1, $N_{control}$=17 cells, 2 mice; $N_{Kv4.3LOF}$=39 cells, 5 mice; and
973 $N_{BKCa1.1LOF}$=13 cells, 3 mice; Ext D1, $N_{control}$=10 cells, 3 mice; $N_{Kv4.3LOF}$=27 cells, 5 mice; and
974 $N_{BKCa1.1LOF}$=23 cells, 3 mice) and average Z-score for dLight1.3b signals in the NAc during FR1
975 day 1 (top) and the first day of extinction (bottom) ($N_{control}$=6; $N_{Kv4.3LOF}$=6; and $N_{BKCa1.1LOF}$=5
976 mice). Comparison of AUC between Day 1 and Day 5 for Z-score action potential firing and
977 dLight1.3b recordings for (**E**) Control (optetrode unpaired Student's *t*-test t_{25}=1.96, P=0.061;
978 dLight1.3b paired Student's *t*-test t_5=4.17, **P<0.01), (**F**) Kv4.3 LOF (optetrode unpaired
979 Student's *t*-test t_{65}=1.83, P=0.072; dLight1.3b paired Student's *t*-test t_5=1.398, P= 0.22) and (**G**)

980 BKCa1.1 LOF (optetrode unpaired Student's *t*-test t_{37}=4.28, **P<0.001, dLight1.3b paired
981 Student's *t*-test t_4=3.34, *P<0.05). Data are presented as mean ± SEM (**B-E**), or Box and Whisker
982 min-to-max graphs (**E-G**).
983
984
985 **Supplementary Materials**
986
987 Supplementary figures.
988

989 References:

990 1. R. A. Wise, Dopamine, learning and motivation. *Nat Rev Neurosci*. **5**, 483–494 (2004).
991 2. W. Schultz, Multiple Dopamine Functions at Different Time Courses. *Annu Rev Neurosci*. **30**, 259–288 (2007).
992 3. H. R. Kim, A. N. Malik, J. G. Mikhael, P. Bech, I. Tsutsui-Kimura, F. Sun, Y. Zhang, Y. Li, M. Watabe-
993 Uchida, S. J. Gershman, N. Uchida, A Unified Framework for Dopamine Signals across Timescales. *Cell*. **183**,
994 1600-1616.e25 (2020).
995 4. M. W. Howe, P. L. Tierney, S. G. Sandberg, P. E. M. Phillips, A. M. Graybiel, Prolonged dopamine signaling
996 in striatum signals proximity and value of distant rewards. *Nature*. **500**, 575–579 (2013).
997 5. A. Mohebi, J. R. Pettibone, A. A. Hamid, J.-M. T. Wong, L. T. Vinson, T. Patriarchi, L. Tian, R. T. Kennedy, J.
998 D. Berke, Dissociable dopamine dynamics for learning and motivation. *Nature*. **570**, 65–70 (2019).
999 6. K. Farrell, A. Lak, A. B. Saleem, Midbrain dopamine neurons provide teaching signals for goal-directed
1000 navigation. *bioRxiv*. **22** (2021).
1001 7. S. W. Johnson, R. A. North, Two types of neurone in the rat ventral tegmental area and their synaptic inputs. *J*
1002 *Physiol* (1992), doi:10.1113/jphysiol.1992.sp019136.
1003 8. F. White, X.- Hu, M. Marinelli, C. Rudick, Excitability of Dopamine Neurons: Modulation and Physiological
1004 Consequences. *CNS Neurol Disord Drug Targets*. **5**, 79–97 (2006).
1005 9. Z. M. Khaliq, B. P. Bean, Dynamic, nonlinear feedback regulation of slow pacemaking by A-type potassium
1006 current in ventral tegmental area neurons. *Journal of Neuroscience*. **28** (2008), doi:10.1523/JNEUROSCI.2237-
1007 08.2008.
1008 10. T. Kimm, Z. M. Khaliq, B. P. Bean, Differential regulation of action potential shape and burst-frequency firing
1009 by BK and Kv2 channels in substantia nigra dopaminergic neurons. *Journal of Neuroscience*. **35** (2015),
1010 doi:10.1523/JNEUROSCI.5291-14.2015.
1011 11. M. E. Soden, G. L. Jones, C. A. Sanford, A. S. Chung, A. D. Güler, C. Chavkin, R. Luján, L. S. Zweifel,
1012 Disruption of Dopamine Neuron Activity Pattern Regulation through Selective Expression of a Human KCNN3
1013 Mutation. *Neuron*. **80** (2013), doi:10.1016/j.neuron.2013.07.044.
1014 12. J. X. Yee, A. Rastani, M. E. Soden, The potassium channel auxiliary subunit Kvβ2 (*Kcnab2*) regulates Kv1
1015 channels and dopamine neuron firing. *J Neurophysiol*. **128**, 62–72 (2022).
1016 13. A. C. Hunker, M. E. Soden, D. Krayushkina, G. Heymann, R. Awatramani, L. S. Zweifel, Conditional Single
1017 Vector CRISPR/SaCas9 Viruses for Efficient Mutagenesis in the Adult Mouse Nervous System. *Cell Rep*
1018 (2020), doi:10.1016/j.celrep.2020.02.092.
1019 14. A. S. Chung, S. M. Miller, Y. Sun, X. Xu, L. S. Zweifel, Sexual congruency in the connectome and translatome
1020 of VTA dopamine neurons. *Sci Rep*. **7** (2017), doi:10.1038/s41598-017-11478-5.
1021 15. P. D. Shepard, B. S. Bunney, Repetitive firing properties of putative dopamine-containing neurons in vitro:
1022 regulation by an apamin-sensitive Ca2+-activated K+ conductance. *Exp Brain Res*. **86** (1991),
1023 doi:10.1007/BF00231048.
1024 16. S. Q. Lima, T. Hromádka, P. Znamenskiy, A. M. Zador, PINP: A new method of tagging neuronal populations
1025 for identification during in vivo electrophysiological recording. *PLoS One*. **4** (2009),
1026 doi:10.1371/journal.pone.0006099.
1027 17. R. Rahamimoff, A. Butkevich, D. Duridanova, R. Ahdut, E. Harari, S. G. Kachalsky, Multitude of ion channels
1028 in regulation of transmitter release. *Philos Trans R Soc Lond B Biol Sci*. **354**, 281–288 (1999).
1029 18. K. J. Burke, K. J. Bender, Modulation of Ion channels in the Axon: Mechanisms and function. *Front Cell*
1030 *Neurosci*. **13** (2019), , doi:10.3389/fncel.2019.00221.
1031 19. N. C. Klapoetke, Y. Murata, S. S. Kim, S. R. Pulver, A. Birdsey-Benson, Y. K. Cho, T. K. Morimoto, A. S.
1032 Chuong, E. J. Carpenter, Z. Tian, J. Wang, Y. Xie, Z. Yan, Y. Zhang, B. Y. Chow, B. Surek, M. Melkonian, V.
1033 Jayaraman, M. Constantine-Paton, G. K. S. Wong, E. S. Boyden, Independent optical excitation of distinct
1034 neural populations. *Nat Methods*. **11** (2014), doi:10.1038/nmeth.2836.
1035 20. J. Wolfart, H. Neuhoff, O. Franz, J. Roeper, Differential expression of the small-conductance, calcium-activated
1036 potassium channel SK3 is critical for pacemaker control in dopaminergic midbrain neurons. *Journal of*
1037 *Neuroscience*. **21** (2001), doi:10.1523/jneurosci.21-10-03443.2001.
1038 21. Z. Niday, B. P. Bean, BK channel regulation of afterpotentials and burst firing in cerebellar purkinje neurons.
1039 *Journal of Neuroscience*. **41** (2021), doi:10.1523/JNEUROSCI.0192-20.2021.
1040 22. J. Clatot, N. Neyroud, R. Cox, C. Souil, J. Huang, P. Guicheney, C. Antzelevitch, Inter-regulation of kv 4.3 and
1041 voltage-gated sodium channels underlies predisposition to cardiac and neuronal channelopathies. *Int J Mol Sci*.
1042 **21** (2020), doi:10.3390/ijms21145057.

1043 23. Z. M. Khaliq, B. P. Bean, Pacemaking in dopaminergic ventral tegmental area neurons: Depolarizing drive from
1044 background and voltage-dependent sodium conductances. *Journal of Neuroscience*. **30** (2010),
1045 doi:10.1523/JNEUROSCI.0143-10.2010.
1046 24. M. E. Soden, A. S. Chung, B. Cuevas, J. M. Resnick, R. Awatramani, L. S. Zweifel, Anatomic resolution of
1047 neurotransmitter-specific projections to the VTA reveals diversity of GABAergic inputs. *Nat Neurosci* (2020),
1048 doi:10.1038/s41593-020-0657-z.
1049 25. B. B. Gore, M. E. Soden, L. S. Zweifel, Manipulating gene expression in projection-specific neuronal
1050 populations using combinatorial viral approaches. *Curr Protoc Neurosci* (2013),
1051 doi:10.1002/0471142301.ns0435s65.
1052 26. A. C. Hunker, L. S. Zweifel, Protocol to Design, Clone, and Validate sgRNAs for In Vivo Reverse Genetic
1053 Studies. *STAR Protoc* (2020), doi:10.1016/j.xpro.2020.100070.
1054 27. F. Wang, J. Flanagan, N. Su, L. C. Wang, S. Bui, A. Nielson, X. Wu, H. T. Vo, X. J. Ma, Y. Luo, RNAscope: A
1055 novel in situ RNA analysis platform for formalin-fixed, paraffin-embedded tissues. *Journal of Molecular*
1056 *Diagnostics*. **14** (2012), doi:10.1016/j.jmoldx.2011.08.002.
1057 28. L. Erben, A. Buonanno, Detection and Quantification of Multiple RNA Sequences Using Emerging
1058 Ultrasensitive Fluorescent In Situ Hybridization Techniques. *Curr Protoc Neurosci*. **87** (2019),
1059 doi:10.1002/cpns.63.
1060 29. J. T. Ting, T. L. Daigle, Q. Chen, G. Feng, Acute brain slice methods for adult and aging animals: Application
1061 of targeted patch clamp analysis and optogenetics. *Methods in Molecular Biology*. **1183** (2014),
1062 doi:10.1007/978-1-4939-1096-0_14.
1063 30. Y. S. Jo, G. Heymann, L. S. Zweifel, Dopamine Neurons Reflect the Uncertainty in Fear Generalization.
1064 *Neuron* (2018), doi:10.1016/j.neuron.2018.09.028.
1065 31. J. M. Ehrich *et al.*, Kappa Opioid Receptor-Induced Aversion Requires p38 MAPK Activation in VTA
1066 Dopamine Neurons. *J Neurosci* **35**, 12917-12931 (2015).
1067 32. R. Spanagel, A. Herz, T. S. Shippenberg, The effects of opioid peptides on dopamine release in the nucleus
1068 accumbens: an in vivo microdialysis study. *J Neurochem* **55**, 1734-1740 (1990).
1069 33. R. Al-Hasani *et al.*, Distinct Subpopulations of Nucleus Accumbens Dynorphin Neurons Drive Aversion and
1070 Reward. *Neuron* **87**, 1063-1077 (2015).
1071 34. S.C. Gantz and B.P. Bean. Cell-Autonomous Excitation of Midbrain Dopamine Neurons by
1072 Endocannabinoid-Dependent Lipid Signaling. *Neuron*. 93, 1375-1387. (2017).
1073 35. R. Gomez, L.F. Maglio, A.J. Gonzalez-Hernandez, B. Rivero-Piréz, D. Bartolomé-Martin, T. Giraldez.
1074 NMDA receptor–BK channel coupling regulates synaptic plasticity in the barrel cortex. *PNAS.* 118 (35) (2021).
1075 36. N.C. Klapoetke *et al.*, Independent Optical Excitation of Distinct Neural Populations. *Nature Methods* **3**, 338-
1076 46 (2014).
1077

1078 **FIGURE 1**

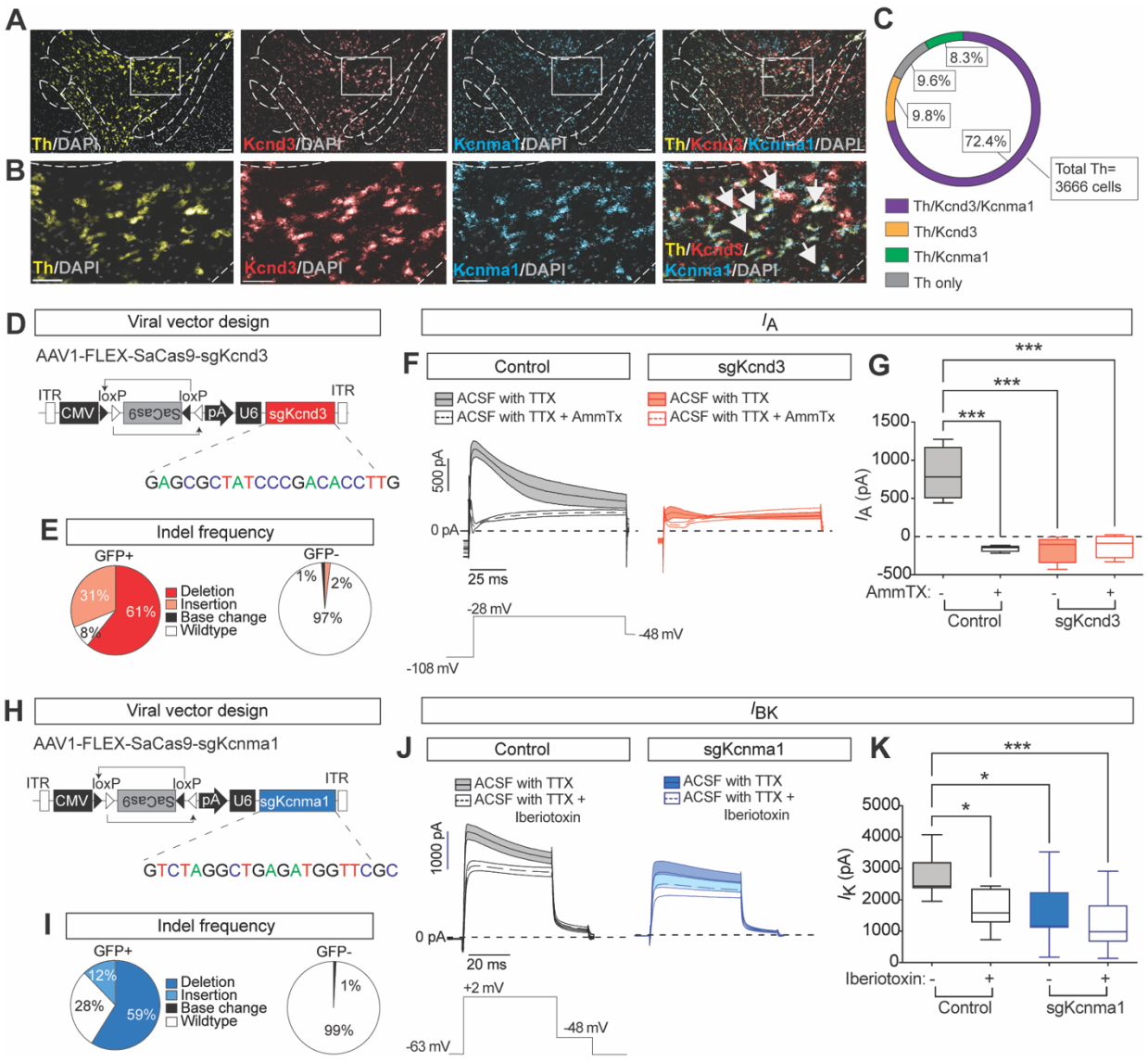

1079
1080

1081 **FIGURE 2**

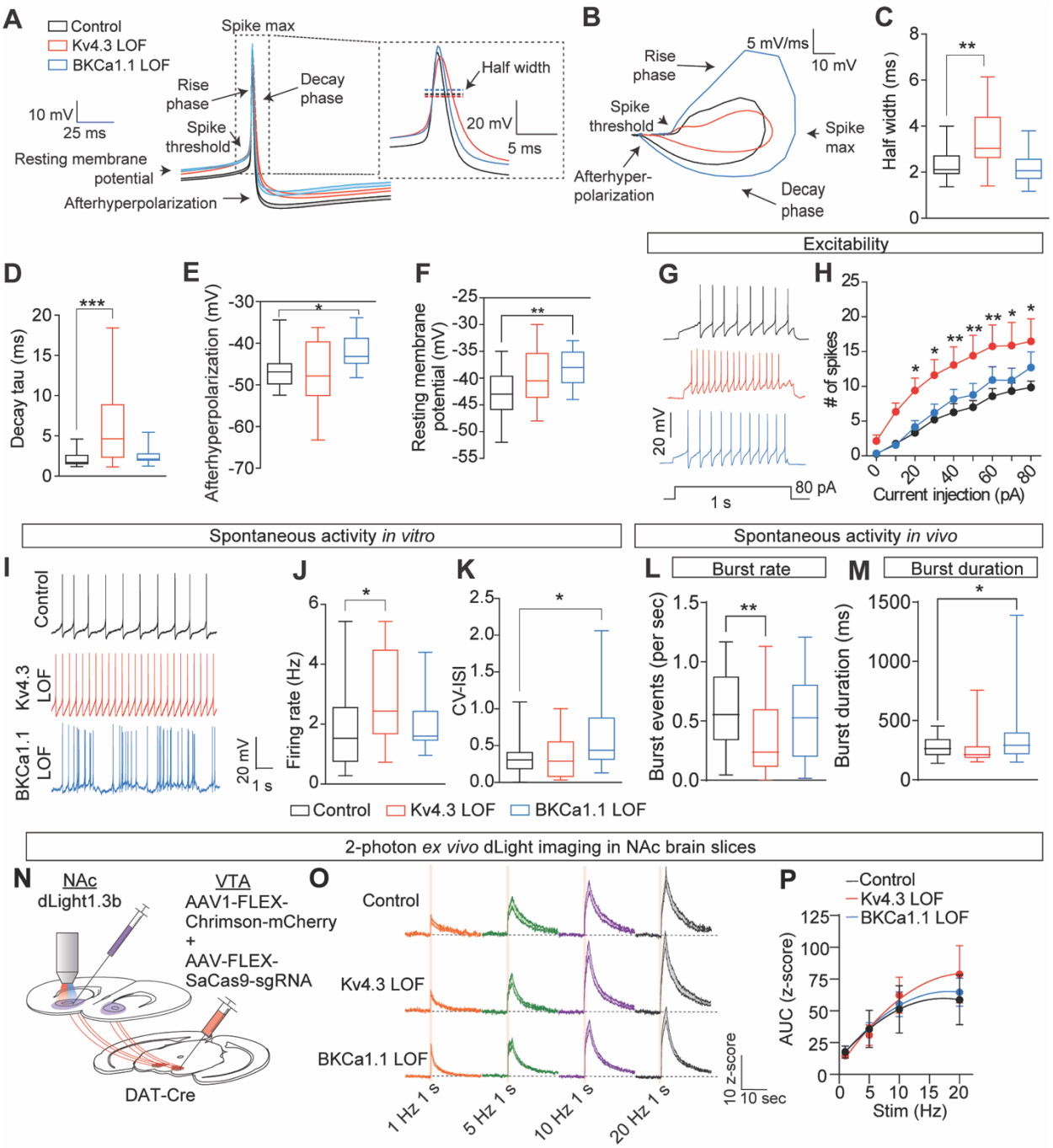

1082
1083

1084 **FIGURE 3**

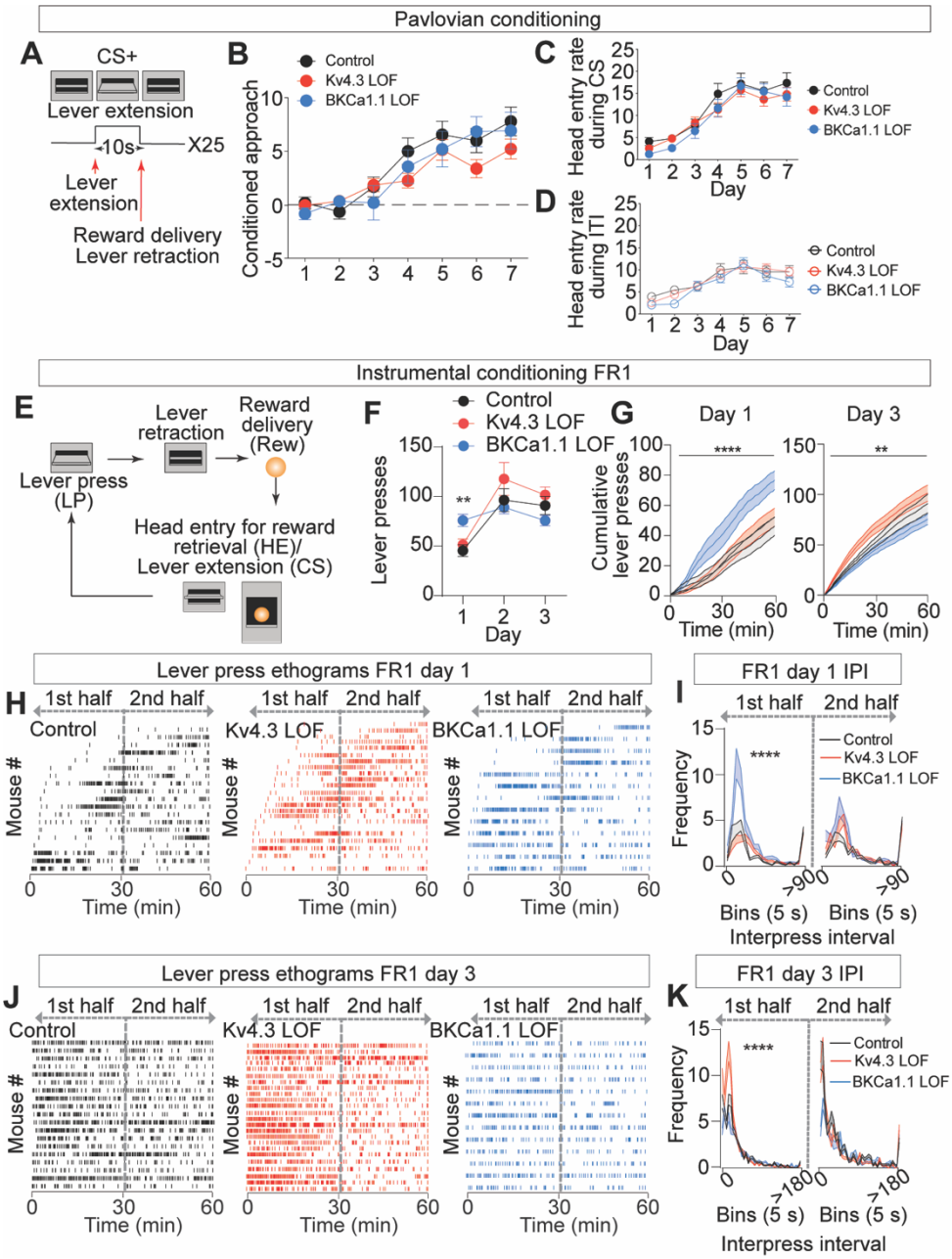

1085
1086

1087 **FIGURE 4**

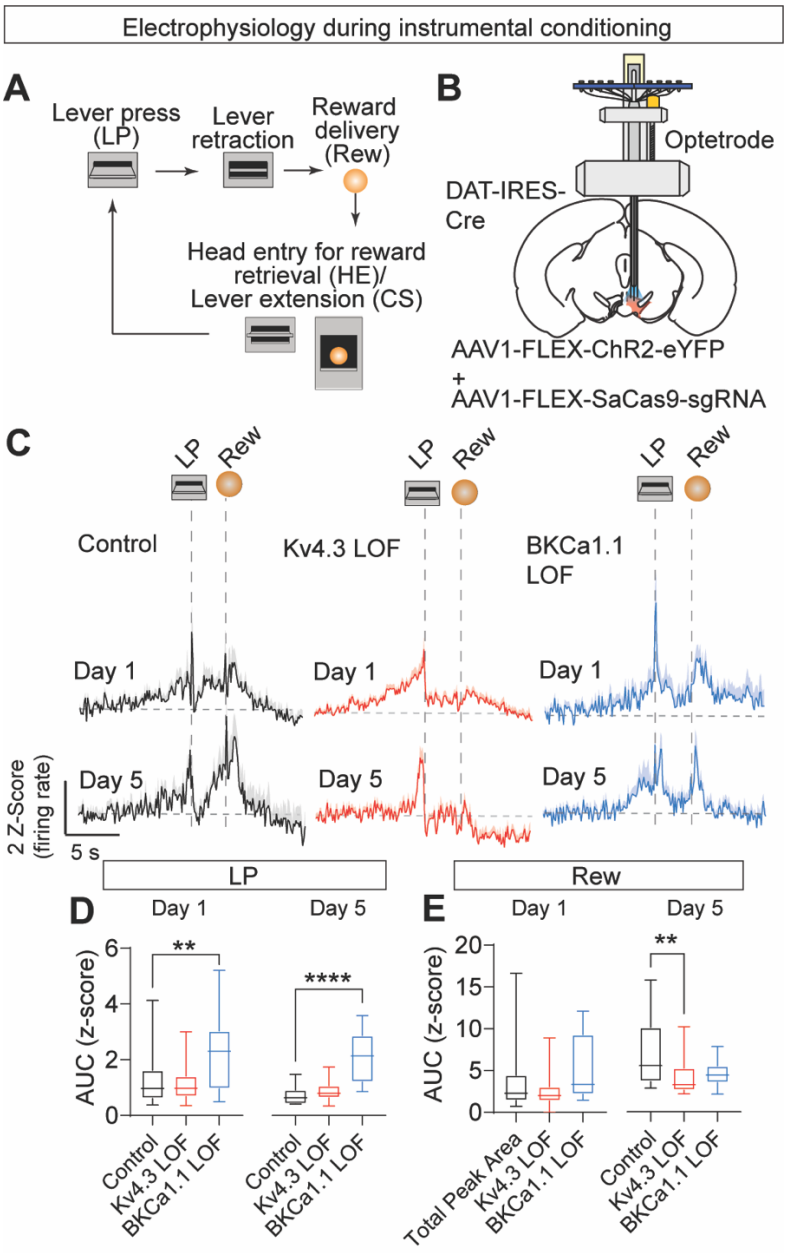

1088
1089

1090 **FIGURE 5**

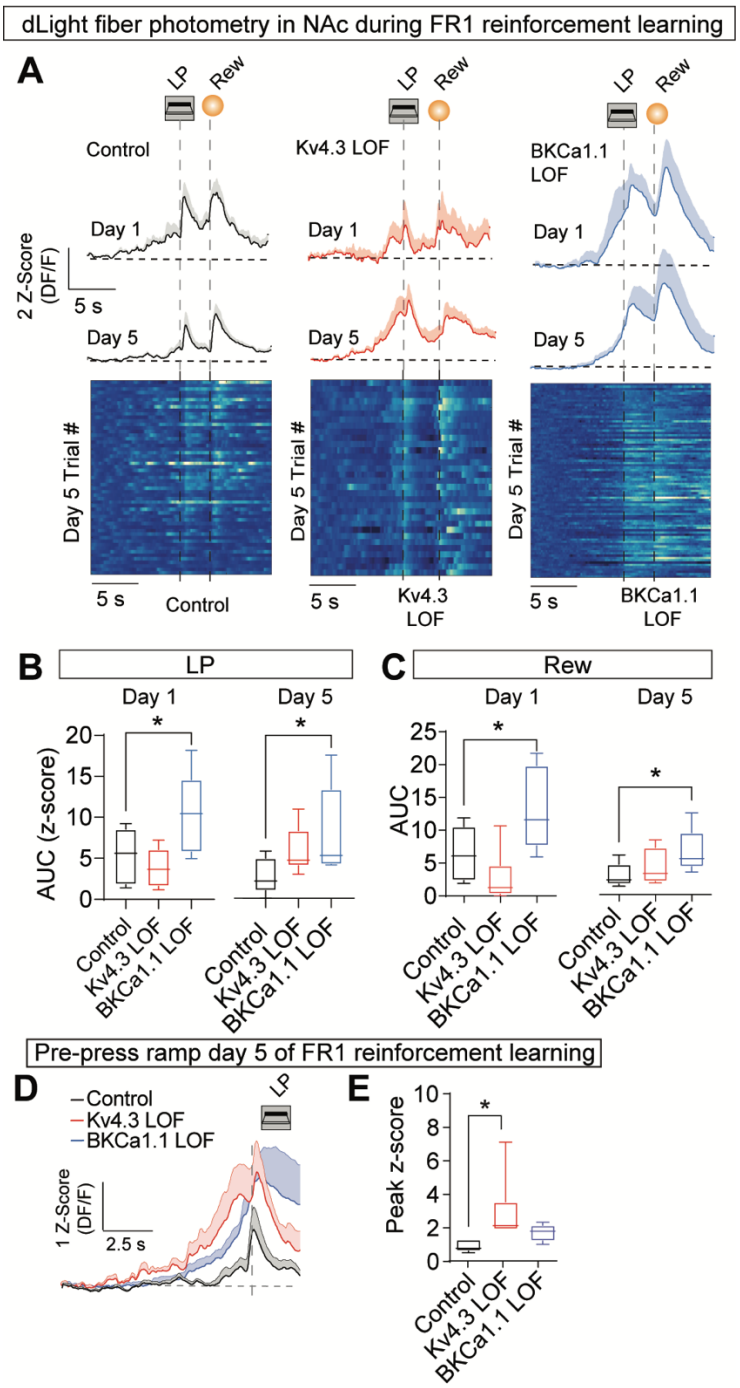

1091
1092

1093 **FIGURE 6**

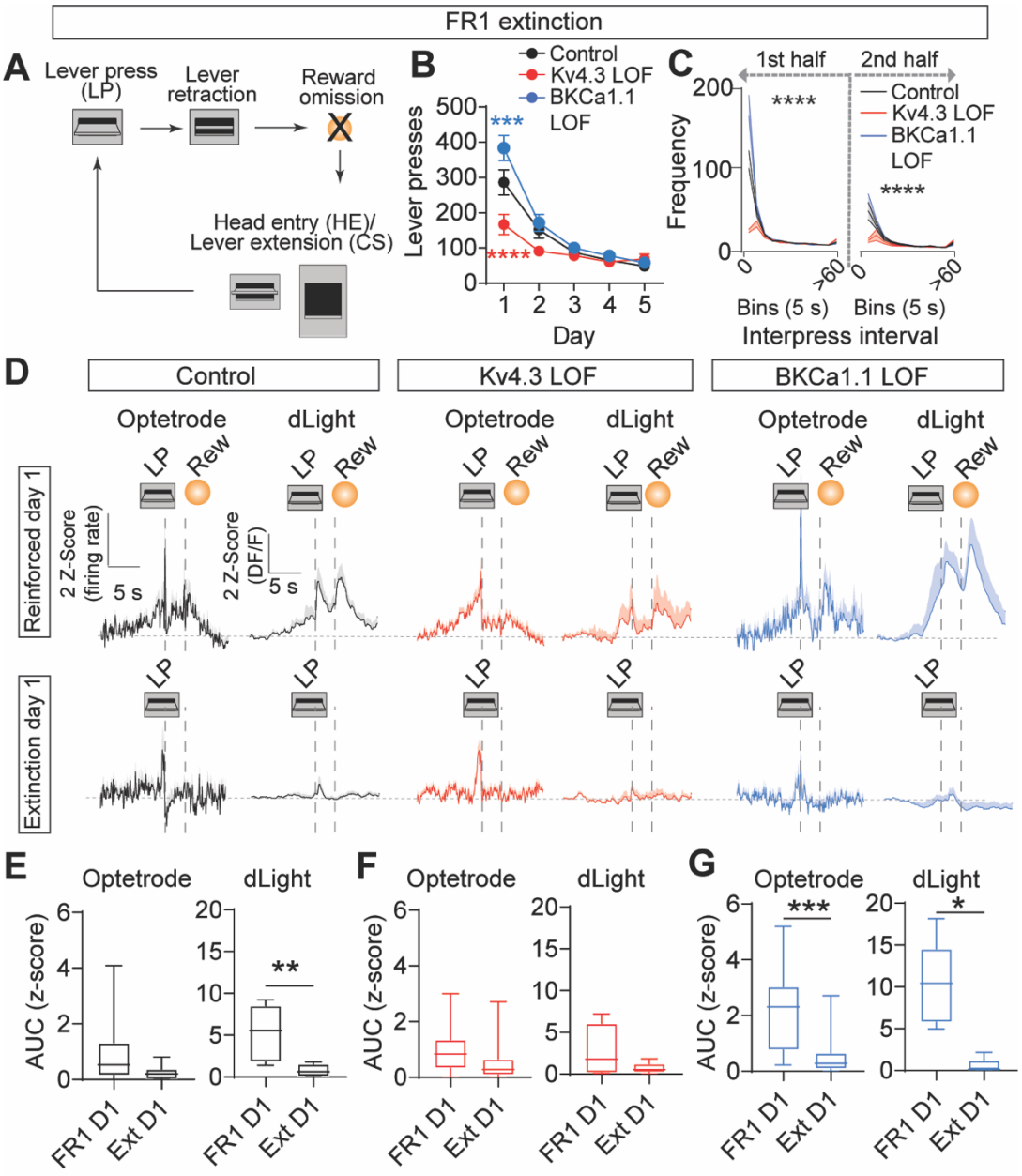

1094
1095